# MODELING AND ANALYSIS OF COVID-19 DYNAMICS WITH INTERVENTION

**Charles Muriuki Wachira**

A Thesis Submitted in Partial Fulfillment of the Requirements for the Award of Degree of Doctor of Philosophy in Applied Mathematics of Masinde Muliro University of Science and Technology.

**November, 2022**

## DECLARATION

This thesis is my original work prepared with no other than the indicated sources and support and has not been presented elsewhere for award of degree or any other award.

Signature..... Date .....

Wachira Charles Muriuki

SEA/H/01-53242/2018

## CERTIFICATION

The undersigned certify that they have read and hereby recommend for acceptance of Masinde Muliro University of Science and Technology a thesis entitled;

"Modeling and Analysis of COVID-19 Dynamics with Intervention"

Signature..... Date .....

Prof. George Lawi,

Department of Mathematics,

Masinde Muliro University of Science and Technology, Kakamega - Kenya.

Signature..... Date .....

Dr. Lawrence Omondi,

Department of Mathematics,

Egerton University - Kenya.

## COPYRIGHT

## DEDICATION

*To everyone who supported this work, my source of inspiration*

## ACKNOWLEDGEMENTS

First, I would like to thank the GOD ALMIGHTY for the gift of life and for providing me with this golden opportunity to complete this work. Prof. G. Lawi and Dr. L. Omondi, my supervisors, I thank you for your supervision, guidance, and constant encouragement to completion of this work. I would also like to thank Dr. A.N. Simiyu and Dr. J.K. Nthiiri for providing me with invaluable teaching opportunities during my graduate studies. Thank you to all the members of the department of mathematics, MMUST for your mentorship and encouragement throughout this incredible journey; you have made my graduate studies so enjoyable. The financial support for my PhD studies came from partial scholarship awarded through the MMUST Merit Scholarship Programme and teaching assistantship in the Department of Mathematics. My heartfelt gratitude also goes to my parents, Jackson and Charity, for their moral support; this work would not have been possible without them. Many thanks to my spouse, family, and relatives for their encouragement and support throughout my studies.

**ABSTRACT**

The coronavirus disease 2019 (COVID-19) is caused by the severe acute respiratory syndrome coronavirus-2 (SARS-CoV-2). The virus is primarily transmitted to humans through inhaling respiratory droplets produced by sneezing, coughing, and conversing closely with an infectious person (direct transmission) or indirectly through contact with contaminated surfaces (indirect transmission). To Prevent and control the fast spreading of COVID-19, health providers and governments around the world have used containment measures such as lockdown, travel bans, cessation of movement, social distancing, proper hygiene, and hand sanitization, among others. Despite these safeguards, the virus continues to spread, although at a slower rate. The disease is linked to a range of infectious periods and human movement (diffusion). Vaccination has proved to be effective in minimising the severity of the disease. Most of the COVID-19 dynamics models so far done have employed a constant coefficient of transmission, whereas infectiousness of an individual varies with time. Thus, an SEIR model is developed to assess the effect of the varying transmission coefficient in the dynamics of COVID-19. The model solutions were checked for well-posedness to ensure that they are both positive and bounded. The next generation matrix approach is applied to determine the effective reproduction number, $R_\omega$. The bifurcation analysis showed that when the transmission coefficient $\beta > \beta^*$ then $R_\omega > 1$ and the disease would spread, otherwise the disease will die out. The numerical simulation showed that reducing the transmission coefficient would curtail the spread of infection. The existing COVID-19 diffusive models do not establish the minimum travelling wave speed that connects the Disease Free Equilibrium (DFE) and the Endemic Equilibrium (EE) enabling infection. Thus, a diffusive COVID-19 model is developed and analyzed to assess the effect of human movement. Existence of travelling wave solutions of the model are shown. Exact solutions to the traveling wave are computed using the Tangent hyperbolic method (Tanh Method). Faced with the inadequate supply of COVID-19 vaccines especially in developing world, it is imperative to determine the critical mass to be vaccinated so as to attain herd immunity. Thus, a COVID-19 model incorporating vaccination is developed and analyzed. Sensitivity analysis done with respect to key parameters of the vaccine reproduction number, $R_V$, indicates that control strategies should target increasing the rate of vaccination with high efficacy vaccines. The study results suggest that a high rate of vaccination ($\gamma$) and high efficacy vaccine ($\vartheta$) are critical in achieving herd immunity also known as 'population immunity' and control disease spread within the population. Optimal control analysis shows that an optimal infection control is achieved by increasing the rate of vaccination and reducing infection by administering a high efficacy vaccine, thus reducing the probability of transmission. Numerical simulations show that when vaccination rates and vaccine efficacy are high, the number of infections fall sharply. The findings of this study highlight the significance of interventions and in particular the specific targets for health care providers in mitigating the transmission of COVID-19.

## TABLE OF CONTENTS

## List of Tables

## List of Figures

## List of Abbreviations

| | | |
|---|---|---|
| **COVID-19** | : | Coronavirus Disease 2019 |
| **WHO** | : | World Health Organization |
| **MOH-K** | : | Ministry of Health Kenya |
| **SIR** | : | Susceptible-Infected-Recovered |
| **SEIR** | : | Susceptible-Exposed-Infected-Recovered |
| **SVEIR** | : | Susceptible-Vaccinated-Exposed-Infected-Recovered |
| **ODE** | : | Ordinary Differential Equations |
| **PDE** | : | Partial Differential Equations |
| $\mathbf{R}_0$ | : | Reproduction Number |
| **DFE** | : | Disease Free Equilibrium |
| **EE** | : | Endemic Equilibrium |
| **MATLAB**$^{TM}$ | : | Mathematics Laboratory |

# CHAPTER ONE

# INTRODUCTION

## 1.1 Background Information

The coronavirus disease 2019 (COVID-19) is a highly contagious respiratory disease caused by the severe acute respiratory syndrome coronavirus-2 (SARS-CoV-2) [37, 38]. COVID-19 is an RNA virus, like flu and measles, that has the ability to mutate [2]. Severe Acute Respiratory Syndrome (SARS) and Middle East Respiratory Syndrome (MERS) viruses are related to COVID-19 [2]. The virus was detected in late December 2019 in Wuhan city, Hubei Province, China. On *March* $11^{th}$, 2020, the World Health Organization (WHO) declared the disease a global pandemic, according to [62, 64]. The epidemic has had a detrimental influence on the economy, society, and health-care systems in almost all countries around the world [2, 4].

It is transmitted through inhalation of respiratory droplets from an infectious person emitted through sneezing, coughing, and having a close conversation, as well as contact with contaminated surfaces [2, 17]. COVID-19 incubation period is the time between virus exposure and onset of symptoms. This is on average 5–6 days, but can be as long as 14 days [35, 65]. The most common COVID-19 symptoms include fever, dry cough, and fatigue. Other symptoms are body ache and pain, sore throat, diarrhoea, headache, loss of taste and smell, difficulties in breathing, rash on skin and discoloration of fingers and toes [17, 18, 45].

Cardiovascular disease, respiratory disease, cancer, and infectious diseases (e.g HIV AIDS, Pneumonia, Influenza, Tuberculosis e.t.c ) are examples of pre-existing conditions, and substance abuse can increase COVID-19 morbidity and mortality [2]. Moreover, pre-existing environmental, demographic conditions (e.g. age, sex, location e.t.c) and socioeconomic conditions (e.g. level of education, income, employment e.t.c) have the potential to influence COVID-19 incidence rate [5]. For example temperature variability influences COVID-19 transmission, such as high humidity and temperature leads to reduced COVID-19 transmission rate [61].

There were no specific antiviral prophylaxis and therapeutics against COVID-19 during the early stages of its outbreak and therefore non-pharmaceutical interventions such as isolation, quarantine, contacts tracing, lockdown and cessation of movement were employed [38]. These interventions were aimed at suppressing and mitigating the epidemic which threatened to overwhelm health-care systems globally. These prevention measures appear to be successful in reducing the number of deaths and hospitalizations [5, 38].

SARS-CoV-2 viral load in the respiratory track peaks at the time of symptom onset or within the first week of illness, then declines. This implies that the most infectious potential exists just before or within the first five days of symptom onset [17]. The role of symptomatic and pre-symptomatic transmission (1-2 days before symptom onset) in the spread of COVID-19 is likely to be greater than that of asymptomatic transmission [18, 51]. This brings into play the idea of a varying transmission coefficient and it would be worthwhile to assess its effects on the dynamics of COVID-19 transmission in humans.

COVID-19 pandemic dynamics are complex in both time and space. These dynamics are caused by a variety of factors, including the spatial distribution of the population's social and economic levels, as well as mobility patterns within a given country [11]. The mobility of individuals from areas with higher COVID-19 prevalence rates exposes individuals in low risk areas to infection. When infected individuals travel to regions that are infection free they might transmit the virus to local residents and cause disease outbreaks. The transfer of infections from a high concentration region to a low concentration region causes a wave of transfer of infection. Equally, movement of susceptible individuals to high risk regions may expose them to contract infection. Restriction of human mobility is considered as an effective strategy to control spreading of the disease. However, it is still unclear whether mobility restriction is a proportional response to control the ongoing COVID-19 pandemic [68]. The purpose of this study is to investigate the impact of human mobility and possibly suggest measures towards reducing the speed of the wave of transfer of infection from high to low risk areas.

Vaccination has been a major public health tool in modern medicine used in minimizing the impact of many infectious diseases of humans [43, 52]. A vaccine is any biologically derived substance that, when administered to a susceptible host, elicits a protective immune response. Vaccines help the body to prepare for disease by taking advantage of the fact that the immunity knows how to defend against infectious organisms, which are typically a virus, bacterium, or toxin [53]. The two vaccination strategies available are mass and ring vaccination. The term "mass vaccination" refers to the immunisation of the entire population, whereas "ring vaccination," also known as "surveillance and containment," refers to the targeted immunisation of primary and secondary contacts. It is a social responsibility choice of an individual to get vaccinated. However, offsetting the fear and adverse side

effects of the vaccine has to be done [27]. If individuals choose not to be vaccinated, they may become infected, which will inflict larger costs for recovery [67].

Currently, vaccines such as BNT162b2 (Pfizer), mRNA1273 (Moderna), ChAd0x1 nCoV-19 (Astra Zeneca), Sputnik, Sinopharm, Johnson & Johnson vaccines among others are being administered worldwide. Vaccines have different efficacy and mechanisms of action [39]. Majority of these vaccines presently have high efficacy and safety levels, which makes them suitable for use in mass vaccination campaigns. Thus, setting up strategies of vaccination became crucial to control the COVID-19 pandemic. Furthermore, vaccination programs may differ across regions due to differences in implementation [4, 14]. For example, some nations were vaccinating their entire population (mass vaccination) and some high risk population (ring/targeted vaccination). The vaccination of a high risk group in a given population may result in herd immunity for entire population. Faced with inadequate supply of COVID-19 vaccines, vaccine hesitancy, and refusal/delay of accepting vaccination [48], what fraction of a country's population should be vaccinated in such a ring/targeted vaccination programme to attain herd immunity?

### 1.2 Statement of the Problem

The continued spreading of COVID-19 posses a threat to human health, irrespective of the preventive and control measures in place. This has inflicted substantial burden on the health sector globally. The movement of infected humans (diffusion) has greatly facilitated the spread of COVID-19. Many countries imposed some interventions such as lockdown, travel restrictions and cessation of movement among others in a bid to minimize the chain of spreading of the virus, with varying degree of success. The existing COVID-19 diffusive models do not establish the minimum travelling wave speed that connects the Disease Free Equilibrium (DFE) and

the Endemic Equilibrium (EE) to enable infection. COVID-19 transmission has exhibited a varying infectiousness which may be attributed to a varying transmission coefficient [17, 57], contrary to the constant transmission coefficient assumed in most studies so far. The inadequate supply of COVID-19 vaccines especially in the developing countries has lead to the implementation of different vaccination strategies leading to different outcomes. Therefore it is imperative to determine the critical mass to be vaccinated so as to attain herd immunity in a given population. This study therefore proposes to develop and analyze COVID-19 dynamics model with intervention (i.e., varying transmission coefficient, diffusion and vaccination).

## 1.3 Research Objectives

### 1.3.1 Main Objective

To develop and analyze a COVID-19 dynamics model with varying transmission coefficient, diffusion, and vaccination.

### 1.3.2 Specific Objectives

The specific objectives of this research study are;

(i) To develop a deterministic COVID-19 dynamics model with varying transmission coefficient and analyze the bifurcation dynamics arising from varying transmission coefficient.

(ii) To develop a diffusive COVID-19 dynamics model and determine the minimum wave speed required for a traveling wave to cause infection.

(iii) To develop a deterministic COVID-19 dynamics model with vaccination to determine the critical mass of individuals to be vaccinated so as to attain herd immunity.

## 1.4 Justification of the Study

COVID-19 outbreak in late December 2019 in the Chinese city of Wuhan sparked global concern. This continued spread of COVID-19 across the world triggered an unprecedented crisis in public health, medical facilities, economic development, and social stability. This study sought to explore the dynamics of COVID-19 under a varying transmission coefficient, which is characteristic of the infection. Furthermore human mobility continues to play a significant role in the transmission of this disease and therefore a diffusive model is appropriate. The optimal analysis with vaccination as a strategy is critical in determining targets for transmission control.

## 1.5 Significance of the Study

The mathematical modelling of viral infection is important in the health sector understanding of transmission dynamics, and prevention and control interventions. A model that incorporates interventions is thus critical in enhancing efforts to reduce the spread of COVID-19 and, eventually, eradicating the viral infection in the population. The findings of this study highlight the significance of interventions and in particular the specific targets for health care providers in mitigating the transmission of COVID-19. Furthermore, the model's formulation and analysis will add to the existing mathematical biology body of knowledge.

## 1.6 Methods of the Study

To achieve the objectives of this study the following methods were used;

(i) COVID-19 dynamics model with varying transmission coefficient ($\beta(x,t)$) is developed and analysed. Bifurcation analysis of the varying transmission coefficient ($\beta(x,t)$) is carried out to determine the nature of the steady states and assess the conditions for the spread of the virus in a given population.

(ii) Diffusive COVID-19 dynamics model is developed and analysed. The diffusive model is presented as partial differential equation (PDE) of the form;

$$\begin{aligned} \frac{\partial N}{\partial t} &= F(N) + D\nabla^2 N \\ &= F(N) + D\frac{\partial^2 N}{\partial x^2} \end{aligned} \tag{1.1}$$

where $N(t,x) = S(t,x) + E(t,x) + I(t,x) + R(t,x)$

and $S(t,x)$, $E(t,x)$, $I(t,x)$ and $R(t,x)$ denote the density of susceptible, exposed, infected and recovered individuals at a location $x \in \Omega \subset \mathbb{R}^n$ and time $t$, respectively, $\Omega$ is open set in region $\mathbb{R}^n$; $F(N)$ represents the transmission dynamics of infection in a population; $D$ is the diffusion coefficient. The symbol $\nabla^2 = \frac{\partial^2}{\partial x^2}$ is the Laplace operator in 1-dimensional space (1-D).

(iii) The vaccination compartment is introduced into the model developed in (i) to determine the critical mass of individuals to be vaccinated so as to attain herd immunity. The rate of vaccination of susceptible population shall be given by $\gamma$ where, $(0 < \gamma \leq 1)$ and the vaccine efficacy parameter is defined by $\vartheta$ where, $0 \leq \vartheta \leq 1$.

(iv) Well-posedness of the model solutions is carried out to show that solutions are positive and bounded. Analysis of the formulated models is done to determine the condition for the spread of the disease in a given population. Data is to be obtained from literature, ministry of health-Kenya (MOH-K) website database.

(v) Numerical simulation of the models are carried out using MATLAB$^{TM}$ software to graphically illustrate the long term behavior of solutions of the models developed in this research.

# CHAPTER TWO

# LITERATURE REVIEW

## 2.1 Introduction

Mathematical models have been used widely in various biological applications such as ecology, population dynamics, tumor growth (cancer), immunology, epidemiology, e.t.c. These models have long been used to generate quantitative data in epidemiology and to provide useful guidelines for outbreak management and policy development [62]. Interest in infectious disease modeling has been revived due to relapse and recurrence of diseases [29]. The pioneers of epidemic modeling Kermack and McKendrick [33], developed an SIR model to explain the dynamics of communicable diseases (e.g., the bubonic plague). This has given birth to modeling frameworks such as the SEIR and SIRS [15]. This chapter provides a review of some mathematical models for COVID-19 disease and other disease-related models that may be useful in this research

## 2.2 Some COVID-19 Epidemiological Models

The study of the distribution, determinants and control of infectious diseases is known as epidemiology [6]. Compartmental models play important role in epidemiological modeling. Such models divide a given population into homogeneous sub-populations. In infectious disease models the individuals in a population are categorized into classes/compartments depending on their status with reference to the disease progression, i.e., susceptible, exposed, infective, or recovered, e.t.c.

An SEIQR (Susceptible-Exposed-Infected-Quarantined-Recovered) model to investigate the spread of COVID-19 is developed and analysed in [8]. The following ODE

system governs the model;

$$\begin{aligned}
\dot{S}(t) &= \Lambda + \nu R - \mu S - \alpha IS - \beta ES, \\
\dot{E}(t) &= \alpha IS + \beta ES - (\delta + \mu)E, \\
\dot{I}(t) &= \delta E - (\mu + \kappa + \omega + \rho)I, \\
\dot{Q}(t) &= \rho I - (\tau + \mu + \sigma)Q, \\
\dot{R}(t) &= \tau Q + \omega I - (\nu + \mu)R.
\end{aligned} \tag{2.1}$$

where " $\cdot$ " denotes the component's derivative with respect to time $t$. $\Lambda$ is the recruitment rate into susceptible class; ($\lambda := \alpha I + \beta E$) is the rate of progression from class $S(t)$ to $E(t)$; $\delta$ is the rate at which an individual develops symptoms; $\rho$ is the rate of quarantine; $\kappa$, is infection induced mortality rate; $\omega$ is the recovery rate without quarantine; $\sigma$ is the disease induced mortality rate among patients who are quarantined, while $\tau$ is the recovery rate of individual in quarantine; $\nu$ is the rate of becoming susceptible again, and $\mu$ is the natural mortality rate. The authors assumed that individuals who are quarantined cannot transmit the virus since they are isolated. The model's disease-free equilibrium point was found to be globally asymptotically stable whenever $R_0 < 1$. It was demonstrated that endemic states exist if the basic reproduction number is greater than unity ($R_0 > 1$). The Routh-Hurwitz criterion and appropriate Lyapunov functions are used to show that the endemic states are asymptotically stable locally and globally, whenever $R_0 > 1$.

The dynamics of COVID-19 disease transmission with two categories of susceptible humans is studied using a deterministic model (i.e., immigrant susceptible and local susceptible) [10]. The model exhibits a globally stable disease-free equilibrium point whenever the basic reproduction number, $R_0 < 1$. For $R_0 > 1$, the endemic equilibrium is also shown to be globally stable. Sensitivity analysis showed that use of personal protective equipments (PPEs) and personal hygiene ($d$), transmis-

sion probability ($\beta$), average number of contacts of infected person per unit time in days ($c$), the rate at which the exposed develop clinical symptoms and the rate of recovery ($\rho$) are important factors to consider in the fight against the spread of COVID-19 infection. The authors recommend implementation of efforts such as quarantine, isolation, travel bans, lock-downs and use of PPEs would curtail the spread of COVID-19.

An $SEQJII_\tau R$ mathematical model for COVID-19 transmission dynamics and control is developed in [63]. The model is represented by the ODE system shown below:

$$\begin{aligned}
\frac{dS}{dt} &= \Lambda - \alpha(1-x)S - \mu S, \\
\frac{dE}{dt} &= \alpha(1-x)S - [\theta(1+y) + \beta + \mu]E, \\
\frac{dQ}{dt} &= \theta(1+y)E - (\eta + \mu)Q, \\
\frac{dJ}{dt} &= \eta Q + \phi(1+z)I - (\mu + \sigma + r + \rho)J, \\
\frac{dI}{dt} &= \beta E - [\phi(1+z) + \lambda + \sigma + \mu]I, \\
\frac{dI_\tau}{dt} &= \gamma J - (\omega + \mu + \sigma)I_\tau, \\
\frac{dR}{dt} &= \gamma I + \rho J + \omega I_\tau - \mu R.
\end{aligned} \tag{2.2}$$

where $\alpha = \frac{\alpha_1 E + \alpha_2 Q + \alpha_3 J + \alpha_4 T + \alpha_5 I_\tau}{N}$ where $x, y, z$ are control parameters. The parameter $x$, is the enlightenment control measure for the susceptible individuals to observe social distance, washing of hands always or the use of hand sanitizer, covering of mouth when talking, coughing and sneezing, $y$ is the enlightenment control measure for exposed individual to be quarantined and $z$ is the enlightenment control measure for the infected individual to be isolated. Both the disease free equilibrium (DFE) and endemic equilibrium (EE) were found to be locally asymptotically stable whenever $R_0 < 1$ and $R_0 > 1$ respectively. The results show that control intervention strategies should target quarantine, isolation, and treatment

rates as such would eliminate the disease from the population with time. Moreover increasing the rates at which the suspected and confirmed cases of COVID-19 are quarantined and isolated respectively reduces the spread of the global pandemic.

A mathematical model is presented in [12]. To effectively control the COVID-19 disease outbreak, an optimal control function is added to the model. The authors incorporate three major control efforts into the model to control the spread: isolation, quarantine, and hospitalisation. These efforts are divided into five functions; $u_1(t)$ denote isolation of the susceptible communities, $u_2(t)$ denote contact track measure by which susceptible individuals with contact history are quarantined, $u_3(t)$ denote contact track measure by which infected individuals are quarantined, $u_4(t)$ denotes control effort of hospitalizing the infected ($I_1$) and $u_5(t)$ denote control effort of hospitalizing the infected ($I_2$). The existence and characterization of optimal control were established using Pontryagin's maximum principle. The DFE and EE were found to be locally asymptotically stable. The findings indicate that implementing the available control measures optimally will significantly reduce infectious populations.

A compartmental mathematical model for analyzing COVID-19 transmission is developed and analyzed in [66]. The authors aimed to explore the optimal control for the novel COVID-19 using non-clinical approach such as lock-downs, frequent hand-wash, use of face mask, and alcohol base hand sanitizer. Sensitivity test was done to obtain the indexes of the parameters of the model. Hamilton and Lagrangian methods were used to investigate the existence of an optimal control. The authors showed that the most active transmission parameters are interposed by introducing control variables.

A mathematical model for the dynamics of COVID-19 is presented in [1]. An optimal control function is added to the model in order to effectively control the outbreak. The main control are; isolation, quarantine, and hospitalization. The result shows that adopting the available control measures to their full potential will greatly reduce infectious populations.

A mathematical model for COVID-19 transmission dynamics and analysis of critical and hospitalized cases with bed requirements is presented in [54]. The model is used to calculate peak magnitude for exposed, asymptomatic infectious, symptomatic infectious, hospitalized, ICUs admissions and number of COVID-19 deaths over time. COVID-19 spread scenario and endpoints of disease are also computed. The infection rate, recovery rate, case fatality rate, and the basic reproduction number are calculated over time. The social distance parameter, various age classes, hospital beds for severe cases, and ICU beds or ventilators for critical cases are all included in the model. The results show that the model would be useful in determining various critical parameters such as daily hospitalisation rates, daily death rates, and the need for normal and ICU beds during peak infection days.

The models so far discussed in this section propose implementation of efforts such as quarantine, isolation, cessation of movement, travel bans and lock-downs to reduce the spread of COVID-19. It is evident that human mobility (diffusion) has a major impact on the dynamics of COVID-19 transmission. Furthermore, the models assumed constant transmission coefficient which is not realistic since ability of COVID-19 infectious person to infect another person change with space and time. Studies have shown that COVID-19 infectiousness is high 2 days prior to symptoms onset and 5 days after symptoms display [17, 18, 19, 51].

## 2.3 Models with Time-dependent Parameters

A rigorous hybrid model and data-driven approach to risk scoring is presented in [34], which is based on a time-varying SIR epidemic model and ultimately each community has a simplified color-coded risk level. The model is represented by the ODE system shown below:

$$\begin{aligned} \frac{dS(t)}{dt} &= -\beta\frac{S(t)I(t)}{N}, \\ \frac{dI(t)}{dt} &= \beta\frac{S(t)I(t)}{N} - \sigma I(t), \\ \frac{dR(t)}{dt} &= \sigma I(t). \end{aligned} \tag{2.3}$$

where $\sigma$, is the recovery rate which is equal to $\frac{1}{D_I}$ denote the average infectious number of days, $\beta$, is the effective contact rate. The authors demonstrated how to calculate this risk score using another useful infection spread metric, $R_t = \frac{\beta_t}{\sigma}$, the time-varying average reproduction number indicating the number of individuals infected would infect in turn. A parameter $\Gamma_t = \frac{I(t).R_t}{D_I.S(t)}$ is introduced denoting the probability of someone currently healthy getting infected in the next 24 hours based on their locality. The approach proposed here allows for quantification of uncertainty in the estimates of $R_t$ and $\Gamma_t$ in the form of confidence intervals.

A poisson model with time-varying transmission and removal rates is presented in [31]. The model is given below;

$$\begin{aligned} \frac{ds(t)}{dt} &= -\beta(t)s(t)i(t), \\ \frac{di(t)}{dt} &= \beta(t)s(t)i(t) - \gamma(t)i(t), \\ \frac{dr(t)}{dt} &= \gamma(t)i(t). \end{aligned} \tag{2.4}$$

where, $\beta(t) > 0$ is the infection's time-varying transmission rate at time $t$, number of infectious contacts per unit time, and $\gamma(t) > 0$ is the time-varying removal

rate at $t$. The reproduction number with respect to time is given as $R_0(t) = \frac{\beta(t)}{\gamma(t)}$. The model accounts for possible random errors in reporting and estimate a time-dependent disease reproduction number $R_0(t)$, which may reflect the effectiveness of virus control strategies. The method is applied to study the pandemic in several severely impacted countries, and analyze and forecast the evolving spread of COVID-19. The authors developed aninteractive web application to help other readers use their method.

A mathematical model that tracks transmission and recovery rates over time $t$ is proposed in [20]. The human population is subdivided into three classes namely; $S(t)$, denotes the numbers of susceptible persons; $X(t)$, the numbers of infected persons and $R(t)$, the numbers of recovered persons at time $t$. The following ODEs govern the model;

$$\begin{aligned} \frac{dS(t)}{dt} &= -\frac{\beta(t)S(t)X(t)}{n}, \\ \frac{dX(t)}{dt} &= \frac{\beta(t)S(t)X(t)}{n} - \gamma(t)X(t), \\ \frac{dR(t)}{dt} &= \gamma(t)X(t). \end{aligned} \tag{2.5}$$

where,

$$S(t) + X(t) + R(t) = n.$$

The transmission rate $\beta(t)$ and recovering rate $\gamma(t)$ are functions of time $t$. The The numerical results show that the one-day prediction errors for the number of infected people $X(t)$ and the number of recovered people $R(t)$ are nearly 3% for the data-set collected. The model can track the transmission rate $\beta(t)$ and the recovering rate $\gamma(t)$ with respect to time $t$, and precisely forecast the COVID-19 outbreak's future trend in China. The authors also examined the independent cascade (IC) model for disease propagation to better understand the impact of social distance. The propagation probabilities in the IC model were linked to the

transmission and recovery rates in the SIR model by the authors. They discovered that social distancing strategies can reduce the effective reproduction number.

The models discussed in this section haven't captured some important demographic and epidemiological parameters (vital dynamics) such as the recruitment rate to the susceptible class, disease induced and natural mortality rates.Furthermore, the virus is exposed to the susceptible individuals (individuals infected but not yet infectious). Therefore it would be important consider a class of exposed individuals, which is absent in the models presented above.

## 2.4 Models Incorporating Diffusion

Reaction-diffusion epidemic models are generally standard epidemic models that assumes that there is movement and interaction of individuals in a given population in space. This implies that there is spatial distribution and interaction of individuals in their physical environs. Human mobility may be due to travel, migration between localities, countries, or towns. A reaction-diffusion equation model is presented as partial differential equations (PDEs) of the form,

$$\frac{\partial u}{\partial t} = F(u) + D\nabla^2 u, \tag{2.6}$$

where $u =: u(t, x)$ represents the density/concentration of state $u$. For instance, $u =: S(x, t)$ represents the susceptible individuals in a position $x \in \Omega \subset \mathbb{R}^n$ at a time $t$, where $\Omega$ is a open set; $F(u)$ represents infection dynamics of an individual occupying a given point $x$ at time $t$; $D$ is the diffusion term that corresponds to mobility of an individual in space, and $\nabla^2$ is the Laplace operator. Many diseases limit the movement of those who are infected, but this is not the case for those who are exposed. Because the exposed are more mobile than the infected, they play a crucial role in disease transmission [56].

A reaction-diffusion model is developed in [38]. The authors described the COVID-19 spread by taking into account the daily average movement of susceptible (S), exposed (E), and asymptomatic individuals ($I_a$). The model was calibrated using data from confirmed infections and deaths in France, as well as their initial spatial distribution. They proposed that only those who are vulnerable, exposed, and asymptotic are moving. The dynamics are governed by a system of three partial differential equations (PDE) and three ordinary differential equations (ODEs), as shown below;

$$\begin{aligned}
\partial_t S - d(t)\Delta S &= -\omega(t)(\beta_e E + \beta_s I_s + \beta_a I_a)\frac{S}{N}, \\
\partial_t E - d(t)\Delta E &= \omega(t)(\beta_e E + \beta_s I_s + \beta_a I_a)\frac{S}{N} - \delta E, \\
\partial_t I_a - d(t)\Delta I_a &= (1-\rho)\delta E - \gamma I_a, \\
I_s^{'} &= \rho\delta E - (\gamma + \mu + \nu) I_s, \\
U^{'} &= \nu I_s - (\gamma + \mu) U, \\
R^{'} &= \gamma(I_a + I_s + U).
\end{aligned} \tag{2.7}$$

where $\mathbf{x} = (x, y) \in \Omega \subset \mathbb{R}^2$, $t > 0$ and the densities of susceptible individual ($S$), exposed individual ($E$), symptomatic infected individual ($I_s$), asymptomatic infected individual ($I_a$), and removed individual ($R$). Parameter estimation is done. The basic reproduction number, $R_0$, is derived. The spatial spread of COVID-19 from March 16 to June 16, 2020 was depicted using numerical simulations based on a combination of level-set and finite differences. The authors compared unlockdown mapping scenarios based on distancing variations or partially spatial lock-downs. The spatial results show that without intervention, the total number of infected is high, and the entirecountry would suffer greatly. Since COVID-19 is spread through contact, population density is an important source of transmission.

A system for parameterizing the bass diffusion model using COVID-19 data is presented in [55]. The principle of system dynamics is used to develop this continuous model. In the powersim simulation tool, the model's parameters are tuned to fit the data using a genetic algorithm. The validation is carried out using standard simulation validation techniques. The input data for the experiments were obtained from publicly accessible databases. The study specifically considered data collected in Austria, France, Italy, South Korea, Slovenia, and Switzerland. The model can be used to make rough estimates with high correlation, but there will be differences between the model and the actual system response. The results show that COVID-19 pandemic's first wave exhibited an S-shaped growth pattern that can substantially be described by the Bass diffusion model.

In the model presented in [28], the authors used Markovian Agents, a flexible modelling technique capable of representing the dynamics of large populations interacting in space and time, to study the evolution of COVID-19 in Italy. The aim was to demonstrate that this modelling approach, which is based on mean field analysis models, performs well in describing the diffusion of phenomena such as COVID-19. The study describes the application of this modelling approach to the Italian scenario, and the results were validated against real data from the official documentation of COVID-19 diffusion in Italy. The outcomes correspond to the major actions taken by the Italian government and their consequences. The study focused on a general diffusion of the infection and does not explore the existence of the travelling wave solutions.

## 2.5 Models Incorporating Vaccination

An epidemiological SEIR-model is presented and analysed in [4]. The authors estimated the parameters of the model that accounts for different severity lev-

els using daily COVID-19 reports from Chicago and NYC from 01-March-2020 to 28-November-2020. The authors used time-dependent model parameters in order to achieve data adherent predictions. The model is used to forecast various vaccination scenarios in which the campaign begins at various times ranging from 01-October-2020 to 01-April-2021.The findings indicate that the earlier the vaccination campaign begins, the greater the potential impact on reducing COVID-19 cases, hospitalizations, and deaths. Furthermore, the rate at which cases, hospitalizations, and deaths increase as vaccination begins later depends heavily on the shape of the infection incidence in each city.

The effect of vaccination frequency and vaccine intrinsic efficacy on COVID-19 prevalence, hospitalizations, and deaths is studied in [39]. To investigate these various scenarios, the authors create a compartmental mathematical model and employ computational methodologies. This enables the identification of some key factors in achieving the vaccination programmes' objectives. The authors used metrics related to the outcomes of the COVID-19 pandemic to assess the impact of vaccine efficacy and vaccine inoculation pace. The rate at which vaccine is administered has a higher impact on reducing the burden of the COVID-19 pandemic. The results show that health institutions should prioritise increasing vaccine inoculation rates and raising public awareness about the importance of COVID-19 vaccines.

In order to estimate the impact of COVID-19 vaccination delays on the number of cases and deaths in Brazil, a mathematical model is formulated in [7]. The authors simulated their model for the populations of the State of Sao Paulo and Brazil as a whole, varying vaccine efficacy and population compliance scenarios. The model predicts that in the absence of vaccination, the number of COVID-19-

related deaths will rise. The findings show that the current delay in vaccination schedules observed in many countries has serious consequences in terms of disease mortality. This should serve as a warning to health officials to expedite the process so that the greatest number of people can be immunized in the shortest amount of time.

Based on the vaccine availability, COVID-19 vaccination strategies differ across countries. Vaccines from Pfizer, Morderna, Oxford AstraZeneca, Sputnik V, Johnson & Johnson, Covaxin, Covishield, and others are being administered globally. Due to an insufficient supply of COVID-19 vaccines, many developing countries are vaccinating only high-risk populations (ring/targeted vaccination). Vaccinating high-risk individuals in a given population may result in herd immunity for the entire population. So, what fraction of a country's population should be vaccinated in such a ring vaccination programme to attain herd immunity?

From literature reviewed above, it is evident that a varying transmission coefficient, an existing vaccination strategy, and human mobility (diffusion) are important factors to consider in the dynamics of COVID-19 transmission. This study therefore proposes to develop and analyze COVID-19 dynamics with intervention (i.e., varying transmission coefficient, diffusion and vaccination). The models developed in this study are in the form of ordinary and partial differential equations.

# CHAPTER THREE

# DYNAMICS OF COVID-19 MODEL WITH VARYING TRANSMISSION COEFFICIENT

## 3.1 Introduction

In this chapter, COVID-19 dynamics model with varying transmission coefficient is developed and analysed. The model is described, formulated, and checked for well-posedness. The steady-state existence and basic reproduction number are computed. Finally, bifurcation, sensitivity, and numerical simulations are carried out. COVID-19 infectiousness is highest within the first five (5) days of symptom onset, after which it decreases. Asymptomatic transmission is less likely to spread SARS-CoV-2 than symptomatic and pre-symptomatic transmission (1-2 days before symptom onset) [18, 51]. Therefore, contrary to the constant transmission coefficient assumed in most previous studies, COVID-19 transmission has exhibited varying transmission coefficient [17, 57]. Therefore, a model with varying transmission coefficient is developed, and its effect on COVID-19 transmission dynamics is investigated.

## 3.2 Model Description and Formulation

Despite the fact that there are underlying conditions that predisposes someone to a higher risk of contracting COVID-19 disease, the population under study is assumed to have an equal level of susceptibility. Individuals in this category are referred to as susceptible individuals, which are denoted by the symbol $S(t)$. When susceptible individuals are exposed to the virus they undergo an incubation period, which is the time between virus exposure and onset of symptoms. This is on average 5–6 days, but can be as long as 14 days [35]. The incubating individuals here in this study are categorised as the exposed class, denoted by $E(t)$. Following the end

of an exposure period, the incubating individuals transit into the infection class denoted by $I(t)$. The infectious potential of COVID-19 is significantly greater just before or within five days of the onset of symptoms [17]. Therefore, the infected class $I(t)$ in this study will include both individuals with and without symptoms. Depending on the severity of the disease symptoms and the intervention strategies in place, the infected individuals may die or recover from the disease. Thus, the class $R(t)$ denotes the number of individuals who have recovered from the infection.

The recruitment of individuals into the susceptible class is through births at the per capita rate $\Lambda$. The susceptible humans become infected through a force of infection $\frac{\beta(x,t)I}{1+\eta I}$, where $\beta$ is the varying transmission coefficient. Following an outbreak, several containment measures are implemented to control the disease's spread. The constant $\eta$, is the half-maximal human saturation constant of the infected individuals in the presence of prevention measures. It is considered to be of Michaelis Menten form to account for saturation of the human infection [60]. The saturated incidence given by $\frac{\beta(x,t)SI}{1+\eta I}$, is reasonable due to the fact that as the infected individuals increase they reach a saturation point. The number of infected individuals decreases as the susceptible population increases due to psychological effects, behavioral changes, or preventive measures taken by the affected individuals [3]. The rate of progression from the exposed to infected class is taken as $\varepsilon$. The rates of natural and disease-induced mortality are $\mu$ and $\delta$, respectively. The recovery rate from the infection is taken as $\lambda$ and $\omega$ is the adherence to ministry of health -Kenya (MOH-K) COVID-19 protocols, where $(0 < \omega < 1)$.

The above model description translates into the following schematic flow diagram.

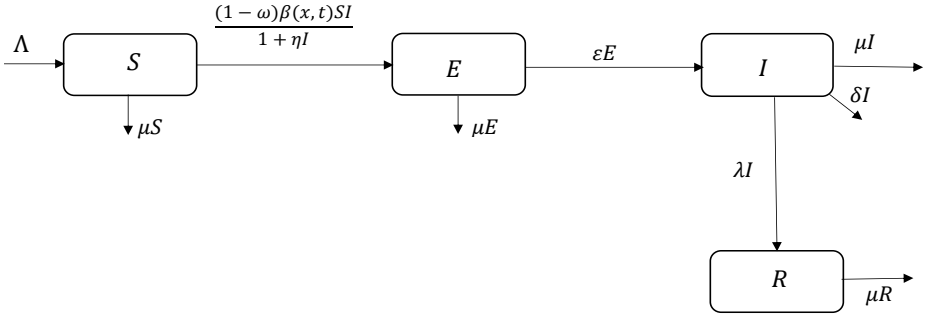


**Figure 3.1: COVID-19 Dynamics Model Schematic Flow Diagram**

From the schematic diagram and description above, proposed model is represented by the following system of ordinary differential equations (odes)

$$\begin{aligned}
\frac{dS}{dt} &= \Lambda - \frac{(1-\omega)\beta(x,t)SI}{1+\eta I} - \mu S, \\
\frac{dE}{dt} &= \frac{(1-\omega)\beta(x,t)SI}{1+\eta I} - (\mu+\varepsilon)E, \\
\frac{dI}{dt} &= \varepsilon E - (\mu+\lambda+\delta)I, \\
\frac{dR}{dt} &= \lambda I - \mu R.
\end{aligned} \tag{3.1}$$

where; $S = S(t), \quad E = E(t), \quad I = I(t), \quad and \quad R = R(t),$

$$\{S, E, I, R\} \in \mathbb{R}^4_+$$

.

**Table 3.1: The Descriptive Summary of the Model Parameters.**

| Parameter | Description | Unit/value units | Source |
|---|---|---|---|
| $\Lambda$ | Recruitment rate | $3.178\times10^{-5}$ day$^{-1}$ | [39] |
| $\mu$ | Natural mortality rate | $3.91\times 10^{-5}$day$^{-1}$ | [7] |
| $\delta$ | Disease mortality rate | $1.03\times 10^{-6}$day$^{-1}$ | [6, 39] |
| $\beta(x,t)$ | Transmission coefficient | (0 - 1.0) day$^{-1}$ | Variable |
| $\omega$ | Adherence to COVID-19 protocols | (0 - 1.0) day$^{-1}$ | Variable |
| $\varepsilon$ | Transition rate from E to I | 0.0877 day$^{-1}$ | [10] |
| $\eta$ | Human saturation constant | 0.05 | Estimated |
| $\lambda$ | Human recovery rate | 0.125 day$^{-1}$ | [25] |

## 3.3 Well-posedness of the Model

In this section well-posedness of the model solutions is discussed. Model (3.1) describes the human population and therefore, its solutions as shown below are positive and bounded for all time $t \geq 0$.

### 3.3.1 Positivity of Solutions

**Proposition 3.3.1.** *Let the initial conditions be*

$$\Omega = \{(S(0), E(0), I(0), R(0)) \geq 0 \in \mathbb{R}^4_+\}.$$

*Then the solutions set*

$$\{S(t), E(t), I(t), R(t)\}.$$

*of model (3.1) are positive* $\forall t \geq 0$.

*Proof.* Considering the first equation in model (3.1), that is

$$\frac{dS}{dt} = \Lambda - \frac{(1-\omega)\beta(x,t)SI}{1+\eta I} - \mu S,$$

where

$$\frac{dS}{dt} \geq -\left[\frac{(1-\omega)\beta(x,t)I}{1+\eta I} + \mu\right] S,$$

integration by variable separation to get

$$\int \frac{dS}{S} \geq \int -\left[\frac{(1-\omega)\beta(x,t)I}{1+\eta I} + \mu\right] dt,$$

thus

$$S(t) \geq S(0)e^{-\left[\int_0^\tau \frac{(1-\omega)\beta(x,\tau)I(\tau)}{1+\eta I(\tau)} + \mu\right] d\tau},$$

which implies that

$$S(t) \geq 0 \ \ \forall t \geq 0.$$

In a similar way, all the other variables can be shown to be positive $\forall t \geq 0$. Hence all solutions of model (3.1) are positive in the region $\Omega$. □

### 3.3.2 Boundedness of Solutions

Model (3.1) is analyzed in a suitable feasible region

$$\Omega = \{(S, E, I, R)(t) \in \mathbb{R}^4_+ : S(t) + E(t) + I(t) + R(t) \leq \frac{\Lambda}{\mu}\}$$

where $S(t) + E(t) + I(t) + R(t) = N(t)$.

Using Proposition 3.3.2 below, the model solutions are shown to be bounded for all $t \geq 0$ in the region $\Omega$.

**Proposition 3.3.2.** *For all time $t \geq 0$, the solutions of model (3.1) are bounded in the region $\Omega$.*

*Proof.* The solutions of model (3.1) are positively invariant of $\Omega$, i.e., all solutions starts in $\Omega$ and remain in the region $\Omega$ for all $t \geq 0$. The rate of change of human population $N(t)$, is given by

$$\frac{dN}{dt} = \frac{dS}{dt} + \frac{dE}{dt} + \frac{dI}{dt} + \frac{dR}{dt},$$

which implies that

$$\begin{aligned} \frac{dN}{dt} &= \Lambda - \mu(S(t) + E(t) + I(t) + R(t)) - \delta I, \\ \frac{dN}{dt} &\leq \Lambda - \mu N, \end{aligned}$$

By variation-of-constant formula, it follows that

$$\limsup_{t\to\infty} N(t) \leq \frac{\Lambda}{\mu},$$

Thus, $N(t) \leq \frac{\Lambda}{\mu}$. This implies that the solution set $\{S(t), E(t), I(t), R(t)\}$ are bounded in the feasible region $\Omega$, i.e,

$$\Omega = \{\{(S(t), E(t), I(t), R(t)\} | S(t) + E(t) + I(t) + R(t) \leq \frac{\Lambda}{\mu}, (S, E, I, R)(0) \geq 0\}.$$

Hence, all solutions of model (3.1) are bounded in the region $\Omega$. □

Clearly, from Proposition 3.3.1 and Proposition 3.3.2 all solutions of model (3.1) are shown to be positively invariant in the region $\Omega$. Thus, model (3.1) is mathematically and epidemiologically well posed in a biological feasible region $\Omega$.

## 3.4 Existence of DFE and the Basic Reproduction Number $R_0$

The model's disease-free equilibrium (DFE) point is defined as the state in which no COVID-19 infection exists in the population under study.

**Proposition 3.4.1.** *The disease-free equilibrium of model (3.1) exists and is given by* $E_0 = (S^0, E^0, I^0, R^0) = (\frac{\Lambda}{\mu}, 0, 0, 0)$.

*Proof.* Let $S \neq 0, E = 0, I = 0$, and $R = 0$ and substituting into the model (3.1) yields

$$\begin{aligned} E_0 &= (S^0, E^0, I^0, R^0), \\ &= (\frac{\Lambda}{\mu}, 0, 0, 0). \end{aligned}$$

which is model (3.1) only disease-free equilibrium point. Therefore, the $DFE$ denoted by $E_0$ is given by $E_0 = (\frac{\Lambda}{\mu}, 0, 0, 0)$. □

### 3.4.1 Reproduction Number

The basic reproduction number, denoted by the symbol $R_0$, is defined as the average number of secondary infections caused by a single infectious individual introduced into a fully susceptible population during his/her period of infectivity [6]. If $R_0 < 1$, then on average an infectious individual produces less than one new infection during the infectious period and hence the infection cannot spread in the population. Conversely, if $R_0 > 1$, then an average infectious individual produces more than a single infection during his/her infectious period and the infection will invade and grow in the population. The next generation matrix method is used to obtain the basic reproduction number [58].

The basic reproduction number $R_0 = \rho(FV^{-1})$, is the spectral radius of the next generation matrix, $FV^{-1}$ where F and V are the matrices of the next generation [58]. The operator $FV^{-1}$, the next generation matrix is constructed from

matrices of partial derivatives of $\mathcal{F}_i$ (rate of appearance of new infection in the $i^{th}$compartment) and $\mathcal{V}_i = \mathcal{V}_i^- - \mathcal{V}_i^+$ (transfer rate/transition rate into and out of the disease compartment $i$) with respect to the infected compartments ($E$ and $I$) evaluated at DFE. The matrices $\mathcal{F}$ and $\mathcal{V}$ are given by

$$\begin{aligned} F &= \left(\frac{\partial \mathcal{F}_i(E_0)}{\partial x_j}\right), \\ V &= \left(\frac{\partial \mathcal{V}_i(E_0)}{\partial x_j}\right), \end{aligned}$$

From the infectious subsystem of model (3.1),

$$\mathcal{F} = \begin{pmatrix} \frac{(1-\omega)\beta(x,t)SI}{1+\eta I} \\ 0 \end{pmatrix},$$

and

$$\mathcal{V} = \begin{pmatrix} (\mu+\varepsilon)E \\ (\mu+\lambda+\delta)I - \varepsilon E \end{pmatrix},$$

Therefore, the transition matrices $F$ and $V$ evaluated at $E_0 = (\frac{\Lambda}{\mu}, 0, 0, 0)$ are;

$$F = \begin{pmatrix} 0 & \frac{(1-\omega)\beta(x,t)\Lambda}{\mu} \\ 0 & 0 \end{pmatrix},$$

and

$$V = \begin{pmatrix} \mu+\varepsilon & 0 \\ -\varepsilon & \mu+\lambda+\delta \end{pmatrix},$$

Then $V$ is invertible and $V^{-1}$ exists, which is given by;

$$V^{-1} = \begin{pmatrix} \frac{1}{\mu+\varepsilon} & 0 \\ \frac{\varepsilon}{(\mu+\varepsilon)(\mu+\lambda+\delta)} & \frac{1}{\mu+\lambda+\delta} \end{pmatrix},$$

and the next generation matrix $FV^{-1}$ is

$$FV^{-1} = \begin{pmatrix} \frac{(1-\omega)\beta(x,t)\varepsilon\Lambda}{\mu(\mu+\varepsilon)(\mu+\lambda+\delta)} & \frac{(1-\omega)\beta(x,t)\Lambda}{\mu(\mu+\lambda+\delta)} \\ 0 & 0 \end{pmatrix},$$

Since intervention measures in this case the adherence to COVID-19 protocols ($\omega$) has been applied the reproduction number is now referred to as the effective reproduction number, denoted by $R_\omega$, where $\rho(FV^{-1})$ is the spectral radius of the next generation matrix, $(FV^{-1})$. Therefore,

$$R_\omega = \frac{(1-\omega)\beta(x,t)\varepsilon\Lambda}{\mu(\mu+\varepsilon)(\mu+\lambda+\delta)}. \tag{3.2}$$

The effective reproduction number, $R_\omega$, is a measure of the severity of an epidemic in the presence of an intervention and one of the most important parameters, determining whether or not the disease will infiltrate a population. This means that if $R_\omega < 1$, the infection is eradicated, whereas if $R_\omega > 1$, the disease will persists in the population and may cause an epidemic.

### 3.5 Bifurcation Analysis of the Model

Bifurcation is the study of how the nature of a dynamical system changes (stability). Local bifurcation occurs when a parameter affects the stability of a dynamical system's equilibrium (fixed) point. Many epidemic models have two equilibrium points: disease free equilibrium (DFE) and endemic equilibrium (EE). The DFE point exists when the effective reproduction number, $R_\omega < 1$ and there exists an endemic equilibrium point when $R_\omega > 1$. In this study, bifurcation analysis is proposed to investigate the effect of varying transmission coefficient on disease occurrence.

Let $\beta^*$ be the bifurcation parameter in equation (3.2). Setting $R_\omega = 1$ and making $\beta^*$ the subject of the formula in equation (3.2) yields

$$\beta^* = \frac{\mu(\mu+\varepsilon)(\mu+\lambda+\delta)}{(1-\omega)\varepsilon\Lambda}. \tag{3.3}$$

The bifurcation values of the transmission coefficient are now computed. When the parameter values in Table 3.1 are substituted into equation (3.3) as $\omega$ is varied, the following results are obtained;

**Case(i)** If $\omega = 0.9$, then $\beta^* = 1.5391$. This means that whenever $\beta > \beta^* = 1.5391$, $R_\omega > 1$ and the disease is endemic, and $\beta < \beta^*$ the disease is eradicated from the population.

**Case(ii)** If $\omega = 0.5$, then $\beta^* = 0.3078$. This means that if $\beta > \beta^* = 0.3078$, then $R_\omega > 1$ and the disease will be endemic, and if $\beta < \beta^* = 0.3078$, the disease will die out in the population.

**Case(iii)** If $\omega = 0.1$, then $\beta^* = 0.1710$. This means that whenever $\beta > \beta^* = 0.1710$, $R_\omega > 1$ and the disease is endemic, and $\beta < \beta^* = 0.1710$ the disease is eradicated from the population.

**Table 3.2: Parameters and their Unit Values used are as follows:**

| **Case** | $\omega$ | $\mu$ | $\Lambda$ | $\varepsilon$ | $\lambda$ | $\delta$ | $\beta^*$ |
|---|---|---|---|---|---|---|---|
| (i) | 0.9 | 0.0000391 | 0.00003178 | 0.087 | 0.125 | 0.00000103 | 1.5391 |
| (ii) | 0.5 | 0.0000391 | 0.00003178 | 0.087 | 0.125 | 0.00000103 | 0.3078 |
| (iii) | 0.1 | 0.0000391 | 0.00003178 | 0.087 | 0.125 | 0.00000103 | 0.1710 |

The bifurcation values of $\beta^*$ as $\omega$ is varied are given in Table 3.2. As shown in cases (i) (ii), and (iii), when the effective reproduction number $R_\omega$ decreases or increases from unity, the DFE and EE change their nature from stable to unstable and vice versa. Depending on the orientation of the bifurcation parameter $\beta^*$, bifurcations can be forward or backward. Forward (supercritical) bifurcation occurs when there is DFE that is locally asymptotically stable whenever $R_\omega < 1$ and the EE is locally asymptotically stable whenever $R_\omega > 1$. which means when the bifurcation parameter is less than the threshold, there are no endemic states. Backward (subcritical) bifurcation occurs when stable disease-free equilibrium and endemic equilibrium coexist whenever $R_\omega < 1$ [22]. Backward bifurcation will be determined by the infectious person's behavior during or after recovery, with the

possibility of reinfection into the susceptible class. Backward bifurcation means there is possible reinfection though $R_\omega < 1$.

Now using the center manifold theory of bifurcation analysis [16, 47], the type of bifurcation at $R_\omega = 1$ is investigated.

**Theorem 3.5.1.** *Consider the general system of ODEs with a parameter* $\beta^*$

$$\frac{dx}{dt} = f(x, \beta^*), \tag{3.4}$$

$f : \mathbb{R} \to \mathbb{R}^n$ *and* $f \in C^2(\mathbb{R}^2 \times \mathbb{R})$ *where* 0 *is the system's equilibrium point and*

*(i)* $A = D_x f(0,0) = \frac{df_i}{dx_i}(0,0)$ *is the linearization matrix of the system given by (3.4) around the point of equilibrium* 0 *with* $\beta^*$ *evaluated at* 0 *Zero is a simple A eigenvalue, and all other A eigenvalues have negative real parts.*

*(ii) The nonnegative right eigenvector u and left eigenvector v of matrix A correspond to the zero eigenvalue.*

*Let* $f_k$ *be the* $k^{th}$ *component of f and*

$$a = \sum_{k,i,j=1}^{n} v_k u_i u_j \frac{\partial^2 f_k}{\partial x_i \partial x_j}(0,0),$$

$$b = \sum_{k,i=1}^{n} v_k u_i \frac{\partial^2 f_k}{\partial x_i \partial \beta^*}(0,0).$$

*The local dynamics of equation (3.4) around the equilibrium point* 0 *are fully determined by the sign of a and b.*

*i. If* $a > 0$, $b > 0$ *when* $\beta^* < 0$ *with* $|\beta^*| \ll 1$, *then* 0 *is locally asymptotically stable and there exists a positive unstable equilibrium; when* $0 < \beta^* \ll 1$, *then* 0 *is unstable and there exists a negative locally asymptotically stable equilibrium.*

*ii. If* $a > 0$, $b < 0$ *when* $\beta^* < 0$ *with* $|\beta^*| \ll 1$, *then* 0 *is unstable, and there exists a locally asymptotically stable negative equilibrium; when* $0 < \beta^* \ll 1$, *then* 0 *is stable, and a positive unstable equilibrium appears.*

*iii. If $a < 0$, $b > 0$ with $|\beta^*| \ll 1$, then 0 is unstable; when $0 < \beta^* \ll 1$, then 0 is locally asymptotically stable, and there exists a positive unstable equilibrium point.*

*iv. $a < 0$, $b > 0$ when $\beta^* < 0$ changes from negative to positive its stability from stable to unstable. Corresponding to a negative unstable equilibrium becomes positive and locally asymptotically stable.*

Let $S = x_1$, $E = x_2$, $I = x_3$, $R = x_4$ and $\beta := \beta^*$. Substituting in the system (3.1), to obtain

$$\begin{aligned}
\frac{dx_1}{dt} &= f_1 = \Lambda - \frac{(1-\omega)\beta^* x_1 x_3}{1+\eta x_3} - \mu x_1, \\
\frac{dx_2}{dt} &= f_2 = \frac{(1-\omega)\beta^* x_1 x_3}{1+\eta x_3} - (\mu+\varepsilon)x_2, \\
\frac{dx_3}{dt} &= f_3 = \varepsilon x_2 - (\mu+\lambda+\delta)x_3, \\
\frac{dx_4}{dt} &= f_4 = \lambda x_3 - \mu x_4.
\end{aligned} \tag{3.5}$$

Using $\beta^*$ as the bifurcation parameter, which occurs $R_\omega = 1$, solving for $\beta^*$ to obtain

$$\beta^* = \frac{\mu(\mu+\varepsilon)(\mu+\lambda+\delta)}{(1-\omega)\varepsilon\Lambda}.$$

Taking $\beta^*$ as a bifurcation value. Evaluating the Jacobian matrix of the system (3.1) at DFE, to obtain $J_{E_0}$ yields

$$J_{E_0} = \begin{bmatrix} -\mu & 0 & -\frac{[(1-\omega)\beta^*\Lambda]}{\mu} & 0 \\ 0 & -(\mu+\varepsilon) & \frac{[(1-\omega)\beta^*\Lambda]}{\mu} & 0 \\ 0 & \varepsilon & -(\mu+\lambda+\delta) & 0 \\ 0 & 0 & \lambda & -\mu \end{bmatrix} \tag{3.6}$$

Two eigenvalues of the Jacobian matrix (3.6) are $\xi_{1,2} = -\mu$, and the other two are obtained from the reduced matrix $A$ given by

$$A = \begin{bmatrix} -(\mu+\varepsilon) & \frac{[(1-\omega)\beta^*\Lambda]}{\mu} \\ \varepsilon & -(\mu+\lambda+\delta) \end{bmatrix} \tag{3.7}$$

The eigenvalues of $A$ are given by

$$\xi_{3,4} = \frac{1}{2}\left[-B \pm \sqrt{B^2 - 4(1-R_0)}\right]$$

where $B = (2\mu + \varepsilon + \lambda + \delta)$

Clearly when $R_\omega = 1$, $J_{E_0}$ has eigenvalues with negative real part and a zero eigenvalue (one eigenvalue of $J_{E_0}$ vanishes). Therefore in such a case, the centre manifold theory is therefore applied. Let the right eigenvector $\vec{u} = (u_1, u_2, u_3, u_4)^T$ associated to the Jacobian $J_{E_0}$ obtained from $(J_{E_0}).\vec{u} = 0$. Hence

$$\begin{aligned} u_1 &= \frac{-(1-\omega)\beta^*\Lambda}{\mu^2}u_3, \\ u_2 &= \frac{(1-\omega)\beta^*\Lambda}{\mu(\mu+\varepsilon)}u_3, \\ u_3 &= u_3, \\ u_4 &= \frac{\lambda}{\mu}u_3. \end{aligned}$$

Again, let the left eigenvector $\vec{v} = (v_1, v_2, v_3, v_4)^T$ associated to $J_{E_0}$ obtained from $(J_{E_0})^T.\vec{v} = 0$, where $(J_{E_0})^T$ is the transpose of $J_{E_0}$. Thus

$$\begin{aligned} v_1 &= 0, \\ v_2 &= \frac{\varepsilon}{(\mu+\varepsilon)}v_3, \\ v_3 &= v_3, \\ v_4 &= \frac{\lambda}{\mu}v_3. \end{aligned}$$

From the property $\vec{u}.\vec{v} = 1$, yields

$$\frac{(1-\omega)\beta^*\Lambda\varepsilon}{\mu(\mu+\varepsilon)^2}u_3v_3 + u_3v_3 + \frac{\lambda^2}{\mu^2}u_3v_3 = 1$$

$$u_3v_3 = \frac{\mu^2(\mu+\varepsilon)^2}{(1-\omega)\beta^*\Lambda\mu\varepsilon + \mu^2(\mu+\varepsilon)^2 + \lambda^2(\mu+\varepsilon)^2}. \tag{3.8}$$

This implies that $u_3 > 0$ if $v_3 > 0$. The non-zero partial derivatives associated with $\mathbf{f} = (f_1, f_2, f_3, f_4)$ at point $E_0$ of system (3.5) are

$$\frac{\partial^2 f_1}{\partial x_1 \partial x_3} = \frac{\partial^2 f_1}{\partial x_3 \partial x_1} = -(1-\omega)\beta^*,$$

$$\begin{aligned}
\frac{\partial^2 f_2}{\partial x_1 \partial x_3} &= \frac{\partial^2 f_2}{\partial x_3 \partial x_1} = (1-\omega)\beta^*, \\
\frac{\partial^2 f_1}{\partial x_3 \partial \beta^*} &= \frac{-(1-\omega)\Lambda}{\mu}, \\
\frac{\partial^2 f_2}{\partial x_3 \partial \beta^*} &= \frac{(1-\omega)\Lambda}{\mu}.
\end{aligned}$$

From the above partial derivatives, since $v_1 = 0$, $a$ and $b$ are given by

$$\begin{aligned}
a &= v_2 u_1 u_3 \frac{\partial^2 f_2}{\partial x_1 \partial x_3}(E_0) + v_2 u_3 u_1 \frac{\partial^2 f_2}{\partial x_3 \partial x_1}(E_0), \\
&= \frac{-2u_3^2 v_3 \varepsilon(\mu+\lambda+\delta)^2}{\Lambda(\mu+\varepsilon)}. \\
b &= u_3 v_2 \frac{\partial^2 f_2}{\partial x_3 \partial \beta^*}(E_0), \\
&= \frac{(1-\omega)\varepsilon\Lambda u_3 v_3}{\mu(\mu+\varepsilon)}.
\end{aligned}$$

Clearly $a > 0$ when $v_3 < 0$ and $b > 0$ when $v_3 > 0$, the following theorem holds:

**Theorem 3.5.2.** *Model (3.1) exhibits a backward bifurcation at $R_\omega = 1$ when $a > 0$ and $v_3 < 0$. A positive unstable endemic equilibrium point exists when $\beta^*$ is zero, and a positive stable equilibrium point exists when $\beta^*$ changes from negative to positive. As a result, given that $v_3 > 0$, the endemic equilibrium point $E^*$ is locally asymptotically stable for $R_\omega > 1$ but close to 1 when $a < 0$.*

### 3.6 Sensitivity Analysis of the Effective Reproduction Number

The sensitivity analysis is performed to determine the effect of the parameters on the effective reproduction number. Sensitive parameters are those that have a significant impact on infection/transmission dynamics. Using the normalised forward sensitivity index from [21]. The model parameter $M$ sensitivity index is given by

$$\Upsilon_M^{R_\omega} = \frac{\partial R_\omega}{\partial M} \times \frac{M}{R_\omega}. \tag{3.9}$$

The effective reproduction number $R_\omega$ of the model (3.1) is given by;

$$R_\omega = \frac{(1-\omega)\beta(x,t)\varepsilon\Lambda}{\mu(\mu+\varepsilon)(\mu+\lambda+\delta)}.$$

The sensitivity indices are;

$$\begin{aligned}
\Upsilon_{\Lambda}^{R_\omega} &= \frac{\partial R_\omega}{\partial \Lambda} \times \frac{\Lambda}{R_\omega} = 1, \\
\Upsilon_{\beta}^{R_\omega} &= \frac{\partial R_\omega}{\partial \beta} \times \frac{\beta}{R_\omega} = 1, \\
\Upsilon_{\omega}^{R_\omega} &= \frac{\partial R_\omega}{\partial \omega} \times \frac{\omega}{R_\omega} = -\frac{\omega}{1-\omega}, \\
\Upsilon_{\mu}^{R_\omega} &= \frac{\partial R_\omega}{\partial \mu} \times \frac{\mu}{R_\omega} = -(1 + \frac{\mu}{\mu+\varepsilon}), \\
\Upsilon_{\varepsilon}^{R_\omega} &= \frac{\partial R_\omega}{\partial \varepsilon} \times \frac{\varepsilon}{R_\omega} = \frac{\mu}{\mu+\varepsilon}, \\
\Upsilon_{\lambda}^{R_\omega} &= \frac{\partial R_\omega}{\partial \lambda} \times \frac{\lambda}{R_\omega} = -\frac{\lambda}{\mu+\lambda+\delta}, \\
\Upsilon_{\delta}^{R_\omega} &= \frac{\partial R_\omega}{\partial \delta} \times \frac{\delta}{R_\omega} = -\frac{\delta}{\mu+\lambda+\delta}.
\end{aligned}$$

Table 3.3 gives a summary of the sensitivity indices of $R_\omega$ evaluated at the baseline parameters values given in Table 3.3.

**Table 3.3: Sensitivity Indices of $R_\omega$ to Model Parameters.**

| **Parameter** | **Description** | **Unit Value** | **Sensitivity index** |
|---|---|---|---|
| $\Lambda$ | Recruitment rate | $3.178\times10^{-5}$ day$^{-1}$ | 1 |
| $\beta(x,t)$ | Transmission coefficient | (0 - 1.0) day$^{-1}$ | 1 |
| $\omega$ | Adherence to COVID-19 protocols | (0 - 1.0) day$^{-1}$ | [-1, 0] |
| $\mu$ | Natural death rate | $3.91\times 10^{-5}$day$^{-1}$ | -1.000449223 |
| $\varepsilon$ | Transition rate from E to I | 0.0877 day$^{-1}$ | 0.000499223 |
| $\lambda$ | Human recovery rate | 0.125 day$^{-1}$ | 0.999679 |
| $\delta$ | Disease mortality rate | $1.03\times 10^{-6}$day$^{-1}$ | -0.000008237 |

From Table 3.3, an increase of the rate of recruitment, $\Lambda$, into the susceptible by 1% and the varying transmission rate $\beta(x,t)$ by 1% would lead to an increase of the value of the effective reproduction number $R_\omega$ by 1%. An increase of the transmission coefficient by unit will increase the effective reproduction number $R_\omega$ by 1%. An increase of the adherence to the ministry of health COVID-19 protocols by unit would reduce the effective reproduction number by 1%. An increase of the natural mortality rate by unit would reduce the effective reproduction number by 1.0003128%. The sensitivity analysis above shows $R_\omega$ is most sensitive to the

per capita recruitment rate, the varying transmission coefficient, and the adherence to M.O.H-K COVID-19 guidelines/protocols, and the natural mortality rate. The sensitivity analysis results proposes that control strategies should target these parameters, so as to curtail the spreading of COVID-19.

### 3.7 Numerical Simulation and Discussion

In this section, the graphical simulation of model (3.1) are presented. The effect of a varying transmission coefficient $\beta$ are investigated through simulations.

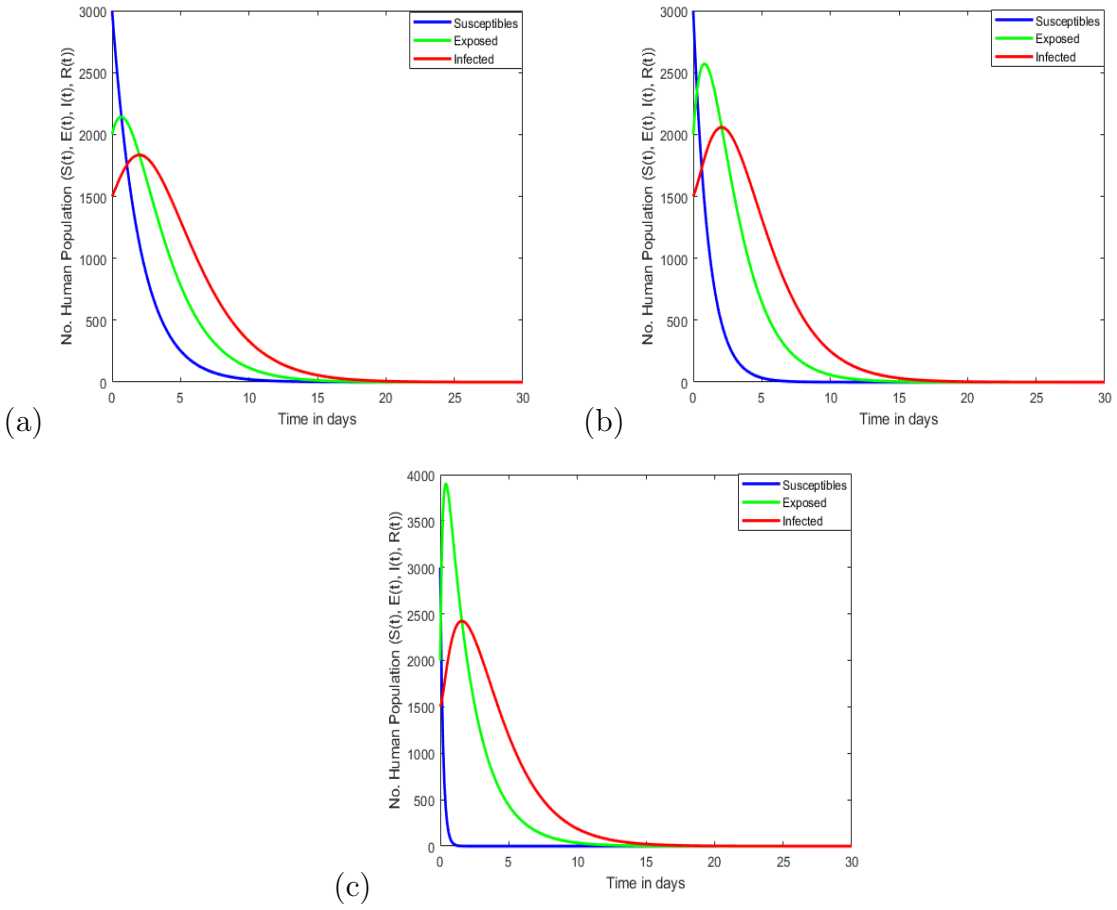


**Figure 3.2: Plots (a), (b), and (c) show varying transmission coefficient $\beta$ at 0.02, 0.09, and 0.5 respectively.**

Figure 3.2, plots (a), (b), and (c) show the dynamics of the susceptible, exposed, infected and recovered humans with varied values of the transmission coefficient $\beta := \beta(x,t)$. It is observed that the susceptible humans reduce with a decrease of $\beta$ and vice versa. When $\beta = 0.5$, the value of $R_\omega$ is given as $R_\omega = 1.624 > 1$, which is greater than unity. When $\beta = 0.09$, the value of $R_\omega$ is given as $R_\omega = 0.2924 < 1$, which is less than unity and when $\beta = 0.02$, the value of $R_\omega$ is given as $R_\omega = 0.06497 < 1$, which is also less than unity. This shows that reducing the transmission coefficient would gradually reduce the population's infection rate. This may be achieved by reducing the interaction between infectious individuals and susceptible population through measures such as maintenance of social distancing, observing personal hygiene, use of face masks, e.t.c.

The varying transmission coefficient $\beta(x,t)$, which varies depending on the population in a given region, plays a critical role in the spread of COVID-19 in different localities within the affected regions. Because of the high rate of infectivity in a region, some parts of the country (particularly densely populated areas) were locked down and movement restrictions was imposed. The study recommends that reducing transmission would optimize the fight against COVID-19 transmission in the population based on the analytical and numerical results obtained. It is concluded that when the transmission coefficient is low, the disease spreading will decrease. This suggests that prevention efforts should focus on lowering the transmission coefficient.

# CHAPTER FOUR

# DYNAMICS OF COVID-19 MODEL WITH DIFFUSION

## 4.1 Introduction

COVID-19 emerged in the city of Wuhan, Hubei Province, China, and quickly spread all over the world [32]. This global spreading was greatly facilitated by movement of infectious individuals from Wuhan city (the epicenter) to other parts of the world where there were no COVID-19 infections. When infected people travel to infection-free areas, the risk of infecting the locals is high and this may result into a spike of infections. Studies have confirmed that COVID-19 dynamics is influenced by human mobility [11]. Diffusion will be defined here as the movement of infectious individuals from a high-risk COVID-19 infection territory to a low-risk area. A diffusive COVID-19 dynamics model with constant transmission coefficient is developed and analysed.

## 4.2 Model Formulation

The transmission dynamics of infectious diseases are influenced by the movement of infectious individuals from one region to another. The movement of individuals from one location to another was ignored in the model (3.1) as in reality individuals are distributed in space and naturally interact with one another. Therefore, diffusivity terms are added to the model (3.1) to investigate the effects of diffusion (human mobility) in COVID-19 transmission dynamics. The existence of travelling wave solutions and their exact solutions of the model are investigated in order to determine the minimum wave speed that may cause an infection. The diffusivity of susceptible, exposed, infected, and recovered individuals are $d_1$, $d_2$, $d_3$, and $d_4$ respectively.

To capture the mobility of individuals in a given population, the following model with spatial diffusion is developed;

$$\begin{aligned}
\frac{\partial S}{\partial t} - d_1\nabla^2 S &= \Lambda - \frac{\beta SI}{1+\eta I} - \mu S, \\
\frac{\partial E}{\partial t} - d_2\nabla^2 E &= \frac{\beta SI}{1+\eta I} - (\mu+\varepsilon)E, \\
\frac{\partial I}{\partial t} - d_3\nabla^2 I &= \varepsilon E - (\mu+\lambda+\delta)I, \\
\frac{\partial R}{\partial t} - d_4\nabla^2 R &= \lambda I - \mu R.
\end{aligned} \tag{4.1}$$

where $\{S(x,t), E(x,t), I(x,t), R(x,t)\} \in \Psi \times T \subset \mathbb{R}^4_+ \times \mathbb{R}$. Human mobility is considered in one-dimensional space i.e., $\nabla^2 = \frac{\partial^2}{\partial x^2}$. The result can be extended into higher-dimensional space, such as 2-dimensional space. It is assumed that susceptible humans are recruited at a constant rate $\Lambda$. Humans who are susceptible to infection are infected by an infectious individual through force of infection $\frac{\beta I}{1+\eta I}$ , where, $\beta$ is the transmission coefficient. The half-maximal human saturation constant of infected individuals is $\eta$. The saturated incidence given by $\frac{\beta SI}{1+\eta I}$, is reasonable due to the fact that as the infected individuals increase they reach a saturation point. The rate of progression from the exposed to infected classes is taken to be $\varepsilon$. The rates of natural and disease-induced mortality are $\mu$ and $\delta$, respectively. The recovery rate from the infection is taken as $\lambda$.

### 4.3 Well-posedness of the Model

The model (4.1) describes human population and therefore its solutions as shown below are positive and bounded for all time $t \geq 0$. The analysis of the model is done under zero flux boundary conditions (no movement across the boundary of $\partial\Psi$).

$$\frac{\partial S}{\partial n} = \frac{\partial E}{\partial n} = \frac{\partial I}{\partial n} = \frac{\partial R}{\partial n} = 0. \tag{4.2}$$

where $\frac{\partial}{\partial n}$, denotes the normal outward derivative on $\partial\Psi$. Let the initial conditions be as follows:

$$S(x,t) = S(x,0) \geq 0, E(x,t) = E(x,0) \geq 0, I(x,t) = I(x,0) \geq 0,$$
$$R(x,t) = R(x,0) \geq 0. \tag{4.3}$$

For $x \in (-\infty, +\infty)$, where $\Psi$ denotes a bounded domain $\Psi \subset \mathbb{R}^4_+$ with smooth boundary $\partial\Psi$ and $t \geq 0$.

**Definition 4.3.1.** *A function $f$ is called **locally Lipschitz continuous** if there exists a neighbourhood $U$ of $x$ for every $x$ in $X$ such that $f$ restricted to $U$ is **Lipschitz continuous** [13].*

**Definition 4.3.2.** *A real-valued function $f : \mathbb{R} \to \mathbb{R}$ is called **Lipschitz continuous** if there exists a positive real constant $K$ such that, for all real $x$ and $y$, then;*

$$|f(x) - f(y)| \leq K|x - y|.$$

**Proposition 4.3.1.** *Suppose that the initial conditions (4.3) hold, then the solutions of model (4.1) are non-negative in [0, $+\infty$) for all $t \geq 0$.*

*Proof.* Model (4.1) can be expressed as an abstract Banach space $X = \bar{C}(\Psi) \times C(\bar{\Psi})$ in the form

$$\begin{aligned} u' &= Au(t) + F(u(t)), \qquad t > 0 \\ u(0) &= u^0 \in X. \end{aligned} \tag{4.4}$$

where $u = (S, E, I, R)^T$, $u(0) = (S(x,0), E(x,0), I(x,0)R(x,0))^T$ and $Au(t) = (d_1 S, d_2 E, d_3 I, d_4 R)^T$ and

$$F(u(t)) = \begin{pmatrix} \Lambda - \frac{\beta SI}{1+\eta I} - \mu S \\ \frac{\beta SI}{1+\eta I} - (\mu + \varepsilon)E \\ \varepsilon E - (\mu + \lambda + \delta)I \\ \lambda I - \mu R \end{pmatrix}. \tag{4.5}$$

Clearly, the function $F$ is locally Lipschitz continuous in $X$, so model (4.1) has local solutions on the interval $[0, T_{max})$, where $T_{max}$ is the maximal existence time for model (4.1) solutions [26].

The model (4.1) can also be written as follows;

$$\begin{aligned} \frac{\partial S}{\partial t} - d_1 \nabla^2 S &= F_1(S, E, I, R), \\ \frac{\partial E}{\partial t} - d_2 \nabla^2 E &= F_2(S, E, I, R), \\ \frac{\partial I}{\partial t} - d_3 \nabla^2 I &= F_3(S, E, I, R), \\ \frac{\partial R}{\partial t} - d_4 \nabla^2 R &= F_4(S, E, I, R). \end{aligned} \tag{4.6}$$

The functions $F_i(S, E, I, R),\ i = 1, 2, 3, 4, 5$ are continuously differentiable and satisfy the following conditions $F_1(0, E, I, R) = \Lambda \geq 0,\ F_2(S, 0, I, R) = 0 \geq 0,$ $F_3(S, E, 0, R) = 0 \geq 0,\ F_4(S, E, I, 0) = 0 \geq 0,$ for all $\{S, E, I, R\} \geq 0$. Since $(S, E, I, R) \geq 0$ with positive initial conditions, then model (4.1) solutions are positive. □

**Proposition 4.3.2.** *Model (4.1) solutions are bounded in the region $\Psi \times T$ for all $t \geq 0$.*

*Proof.* To check for the boundedness, adding all the equations in (4.1) and setting $D = \max\{d_1, d_2, d_3, d_4\}$ to obtain

$$\frac{\partial N(x,t)}{\partial t} \leq \Lambda - \mu N + D\nabla^2 N, \tag{4.7}$$

The inequality (4.7) has a unique solution of the form

$$\frac{\partial N(x,t)}{\partial t} \leq \Lambda - \int_{-\infty}^{\infty} \frac{\mu N}{\sqrt{4D\pi t}} e^{\frac{(-x^2)}{4Dt}} dx, \tag{4.8}$$

where the fundamental solution of inequality (4.8) is given by

$$K(x,t) = \begin{cases} \frac{1}{\sqrt{4D\pi t}} e^{(\frac{-x^2}{4Dt})} & x \in \mathbb{R} \qquad t > 0 \\ \\ 0 \qquad\qquad\qquad\quad x \in \mathbb{R} \qquad t < 0 \end{cases} \tag{4.9}$$

The one-dimensional reaction-diffusion equation (4.9) satisfies the following conditions.

$$K(x,t) = \int_{-\infty}^{+\infty} \frac{1}{\sqrt{4D\pi t}} e^{(\frac{-x^2}{4Dt})} dx = 1, \tag{4.10}$$

Hence

$$\frac{dN}{dt} \leq \Lambda - \mu N, \tag{4.11}$$

Since $N(x,t) > 0$, solving the inequality (4.11) and taking the limit as $t \to \infty$ yields

$$\limsup_{t\to\infty} N(x,t) \leq \frac{\Lambda}{\mu}. \tag{4.12}$$

Hence $N(x,t)$ is bounded. □

From Proposition 4.3.1 and Proposition 4.3.2, it is clear that model (4.1) solutions are positive and bounded for $t \geq 0$. Thus, model (4.1) is mathematically and epidemiologically meaningful, and it is now sufficient to consider its solutions in $\Psi \times T$.

## 4.4 Basic Reproduction Number and the Existence of Equilibrium Points

Following the steps as shown in section 3.4.1 the basic reproduction number of model (4.1) without diffusion is given by;

$$R_0 = \frac{\beta\varepsilon\Lambda}{\mu(\mu+\varepsilon)(\mu+\lambda+\delta)}. \tag{4.13}$$

**Proposition 4.4.1.** *Model (4.1) has a disease free equilibrium denoted by* $E_0 = (S^0, E^0, I^0, R^0) = \{\frac{\Lambda}{\mu}, 0, 0, 0\}$ *where* $S^0 = \frac{\Lambda}{\mu}$, $E^0 = I^0 = R^0 = 0$.

*Proof.* In model (4.1) setting $S \neq 0$, $E = 0$, $I = 0$ and $R = 0$ yields

$$\begin{aligned} E_0 &= \{S^0 = \frac{\Lambda}{\mu}, E^0 = 0, I^0 = 0, R^0 = 0\}, \\ &= \{\frac{\Lambda}{\mu}, 0, 0, 0\}. \end{aligned}$$

which is the only disease-free equilibrium of the model (4.1). □

The endemic equilibrium is the state at which the disease remains persistence in a given population.

**Proposition 4.4.2.** *The endemic equilibrium $E_*$ of the model (4.1) exists whenever $R_0 > 1$.*

*Proof.* The endemic equilibrium exists, if $I^* > 0$ whenever $R_0 > 1$. Consider an endemic equilibrium $E_* = \{S^*, E^*, I^*, R^*\}$ satisfying;

$$\begin{aligned} \Lambda - \frac{\beta S^* I^*}{1+\eta I^*} - \mu S^* &= 0, \\ \frac{\beta S^* I^*}{1+\eta I^*} - (\mu+\varepsilon)E^* &= 0, \\ \varepsilon E^* - (\mu+\lambda+\delta)I^* &= 0, \\ \lambda I^* - \mu R^* &= 0. \end{aligned} \tag{4.14}$$

where $\{S^* \neq 0, E^* \neq 0, I^* \neq 0, R^* \neq 0\}$.

From the first equation of model (4.14) obtains

$$S^* = \frac{\Lambda(1+\eta I^*)}{\beta I^* + \mu(1+\eta I^*)}. \tag{4.15}$$

substituting equation (4.15) into second equation of (4.14) yields

$$E^* = \frac{\beta \Lambda I^*}{(\mu+\varepsilon)(\beta I^* + \mu(1+\eta I^*))}. \tag{4.16}$$

Now substituting equation (4.16) into the third equation of (4.14) yields

$$I^* = \frac{\mu(R_0-1)}{\beta+\mu\eta}. \tag{4.17}$$

It is clear from equation (4.17) that $I^* > 0$ when $R_0 > 1$. This implies that there exists an endemic equilibrium for model (4.1) whenever $R_0 > 1$. □

## 4.5 Spatial Dynamics Analysis

In this section, the model (4.1) is analysed to investigate the spatial dynamics of COVID-19 disease transmission dynamics. The approach used in [40, 41], is employed to determine the existence of travelling wave solutions and seek to determine the speed at which COVID-19 infection spreads in a population.

### 4.5.1 Existence of the Travelling Wave Solutions

Traveling wave solutions are solutions with a specific shape that incorporate time and spatial variables via moving coordinates. The spatial transition from one steady state to another is described by such a solution. The goal of this section is to determine the traveling wave fronts that connect the disease-free and endemic stable states. The travelling wave solution of the model (4.1) is determined following the approach used in [40]. The travelling wave solutions of model (3.1) are shown using the approach used in [40, 59].

**Proposition 4.5.1.** *For all time $t \geq 0$ and $v > 0$, then there exists a traveling wave solutions of model (4.1).*

*Proof.* Define a new variable of the form $z = k(x - vt)$, $v > 0$, where $v$ is the propagating wave speed of model (4.1) in one-dimensional space and $k$ is the wave number. Let $S(x,t) = S(z), E(x,t) = E(z), I(x,t) = I(z)$, and $R(x,t) = R(z)$. Then model (4.1) can be transformed into the following set:

$$\begin{aligned} -vkS^{'} - d_1k^2S^{''} &= \Lambda - \frac{\beta SI}{1+\eta I} - \mu S, \\ -vkE^{'} - d_2k^2E^{''} &= \frac{\beta SI}{1+\eta I} - (\mu+\varepsilon)E, \\ -vkI^{'} - d_3k^2I^{''} &= \varepsilon E - (\mu+\lambda+\delta)I, \\ -vkR^{'} - d_4k^2R^{''} &= \lambda I - \mu R. \end{aligned} \tag{4.18}$$

where $'$ denotes the partial derivative with respect to the new variable $z$. System (4.18) can be expressed as follows;

$$\begin{aligned} d_1k^2S^{''} + vkS^{'} + \Lambda - \frac{\beta SI}{1+\eta I} - \mu S &= 0, \\ d_2k^2E^{''} + vkE^{'} + \frac{\beta SI}{1+\eta I} - (\mu+\varepsilon)E &= 0, \\ d_3k^2I^{''} + vkI^{'} + \varepsilon E - (\mu+\lambda+\delta)I &= 0, \\ d_4k^2R^{''} + vkR^{'} + \lambda I - \mu R &= 0. \end{aligned} \tag{4.19}$$

which can further be expressed as

$$\begin{aligned} S^{''} + H_1 S^{'} + F_1(S, E, I, R) &= 0, \\ E^{''} + H_2 E^{'} + F_2(S, E, I, R) &= 0, \\ I^{''} + H_3 I^{'} + F_3(S, E, I, R) &= 0, \\ R^{''} + H_4 R^{'} + F_4(S, E, I, R) &= 0, \end{aligned} \tag{4.20}$$

where

$$F_1 = \frac{1}{d_1 k^2}(\Lambda - \frac{\beta SI}{1+\eta I} - \mu S), \qquad F_2 = \frac{1}{d_2 k^2}(\frac{\beta SI}{1+\eta I} - (\mu + \varepsilon))E,$$

$$F_3 = \frac{1}{d_3 k^2}(\varepsilon E - (\mu + \lambda + \delta)I), \qquad F_4 = \frac{1}{d_4 k^2}(\lambda I - \mu R).$$

and

$$H_i = \frac{v}{d_i k}, \qquad i = 1, 2, 3, 4$$

Setting the variables $x_1 = S^{'}$, $x_2 = E^{'}$, $x_3 = I^{'}$, $x_4 = R^{'}$, then model (4.20) is transformed into a system of first order differential equations:

$$Y = [x_1, S, x_2, E, x_3, I, x_4, R] \in \mathbb{R}^8$$

and

$$\frac{dY}{dz} = f(Y) = \begin{bmatrix} -H_1 x_1 - F_1 \\ x_1 \\ -H_2 x_2 - F_2 \\ x_2 \\ -H_3 x_3 - F_3 \\ x_3 \\ -H_4 x_4 - F_4 \\ x_4 \end{bmatrix}, \tag{4.21}$$

with boundary conditions

$$\lim_{z \longrightarrow -\infty} (x_1, S, x_2, E, x_3, I, x_4, R) = E_0,$$

$$\lim_{z \longrightarrow +\infty} (x_1, S, x_2, E, x_3, I, x_4, R) = E_*.$$

where $E_0$ denotes the disease-free equilibrium point and $E_*$ denotes the endemic equilibrium point A travelling wave solution is then a trajectory that connects $E_0$ and $E_*$.

Computing the Jacobian matrix of model (4.20) yields

$$J = \begin{bmatrix} -H_1 & -\frac{1}{d_1k^2}(\frac{\beta I}{(1+\eta I)} - \mu) & 0 & 0 & 0 & -\frac{1}{d_1k^2}\frac{\beta S}{(1+\eta I)^2} & 0 & 0 \\ 1 & 0 & 0 & 0 & 0 & 0 & 0 & 0 \\ 0 & -\frac{1}{d_2k^2}\frac{\beta I}{(1+\eta I)} & -H_2 & \frac{(\mu+\varepsilon)}{d_1k^2} & 0 & -\frac{\beta S}{d_2k^2(1+\eta I)^2} & 0 & 0 \\ 0 & 0 & 1 & 0 & 0 & 0 & 0 & 0 \\ 0 & 0 & 0 & \frac{\varepsilon}{d_3k^2} & -H_3 & \frac{(\mu+\lambda+\delta)}{d_3k^2} & 0 & 0 \\ 0 & 0 & 0 & 0 & 1 & 0 & 0 & 0 \\ 0 & 0 & 0 & 0 & 0 & \frac{\lambda}{d_4k^2} & -H_4 & \frac{\mu}{d_4k^2} \\ 0 & 0 & 0 & 0 & 0 & 0 & 1 & 0 \end{bmatrix} \tag{4.22}$$

Evaluating the Jacobian in equation (4.22) at the Disease-free equilibrium $E_0 = (\frac{\Lambda}{\mu}, 0, 0, 0, 0)$ yields

$$J_{E_0} = \begin{bmatrix} -\frac{v}{d_1k} & \frac{\mu}{d_1k^2} & 0 & 0 & 0 & \frac{\beta\Lambda}{\mu d_1k^2} & 0 & 0 \\ 1 & 0 & 0 & 0 & 0 & 0 & 0 & 0 \\ 0 & 0 & -\frac{v}{d_2k} & \frac{(\mu+\varepsilon)}{d_2k^2} & 0 & -\frac{\beta\Lambda}{\mu d_2k^2} & 0 & 0 \\ 0 & 0 & 1 & 0 & 0 & 0 & 0 & 0 \\ 0 & 0 & 0 & \frac{\varepsilon}{d_3k} & -\frac{v}{d_3} & \frac{(\mu+\lambda+\delta)}{d_3k^2} & 0 & 0 \\ 0 & 0 & 0 & 0 & 1 & 0 & 0 & 0 \\ 0 & 0 & 0 & 0 & 0 & \frac{\lambda}{d_4k^2} & -\frac{v}{d_4k} & \frac{\mu}{d_4k^2} \\ 0 & 0 & 0 & 0 & 0 & 0 & 1 & 0 \end{bmatrix} \tag{4.23}$$

The eigenvalues of the Jacobian matrix (4.23) evaluated at the disease-free equilibrium, $\xi_1, ..., \xi_8$ are:

$$\begin{aligned} \xi_{1,2} &= \frac{-v \pm \sqrt{v^2 + 4\mu d_1}}{2d_1k}, \\ \xi_{3,4} &= \frac{-v \pm \sqrt{v^2 + 4(\mu+\varepsilon)d_2}}{2d_2k}, \\ \xi_{5,6} &= \frac{-v \pm \sqrt{v^2 + 4(\mu+\lambda+\delta)d_3}}{2d_3k}, \\ \xi_{7,8} &= \frac{-v \pm \sqrt{v^2 + 4\mu d_4}}{2d_4k}. \end{aligned} \tag{4.24}$$

Clearly, $\xi_1, ..., \xi_8$ are real-valued eigenvalues. Therefore, the travelling wave solutions have real eigenvalues if $v > 0$ for all $t \geq 0$. Model (4.1) has travelling wave

solutions which propagate at a speed $v > 0$, joining the DFE to EE. □

There is a travelling wave profile that connects the disease-free and endemic equilibrium. In epidemiological terms, this means that if infectious individuals are introduced into a susceptible population, a transition zone of infectious individuals will form, propagating at minimum speed $v_{min} := v^*$, where $v \geq v^*$.

### 4.5.2 Exact Solutions of the Traveling Wave

In this section the exact solution of the traveling wave is investigated. To find the exact solution of wave propagation, the Hyperbolic Tangent Method (Tanh Method) is used. In comparison to other existing techniques, the method is concise and straightforward [41]. The Tanh method was first described in [42]

The tanh method is used in the following steps:

1. To find solitary wave solutions to the nonlinear partial differential equation of form

$$u_t = F(u, u_{xx}, ...), \tag{4.25}$$

The solution to equation (4.25) is proposed to be a polynomial

$$F(W) = \sum_{n=0}^{N} a_n W^n, \tag{4.26}$$

A travelling wave solution would use the coordinates $z = k(x - vt)$ and $u(x,t) = u(z)$, where $u(z)$ represents the localised, wave solution with velocity $v$ [41]. Consequently, the given PDEs are transformed into ODEs (*see in equations (4.18) and (4.19)*)

2. The center step is to introduce $W = tanh(z)$ as a new independent variable, and the derivatives are then changed to:

$$W' = sech^2(z) = 1 - tanh^2(z) = 1 - W^2, \tag{4.27}$$

$$\frac{dF(W)}{dz} = (1 - tanh^2(z))\frac{dF(W)}{dW} = (1 - W^2)\frac{dF(W)}{dW}, \tag{4.28}$$

$$\frac{d^2F(W)}{dz^2} = (1 - W^2)\frac{d}{dW}\left[(1 - W^2)\frac{dF(W)}{dW}\right]. \tag{4.29}$$

The degree of the polynomial is then determined as in equation(4.26) by equating each of the equation's two highest exponents to obtain a linear system for $N$, and that system is then solved by rejecting any solution $N$ that is not a positive integer [41].

3. After determining the degree of the polynomial and its coefficients, $a_n$, $n = 0, 1, 2, ..., N$, the nonlinear system is solved using the following assumptions:

- All of the parameters in the problem are strictly positive.
- The coefficient of the highest power of $W$ term must be non-zero.
- The wave number $k$ is considered to be positive.

4. Finally, the coefficients and parameters solutions are substituted into the original equation.

Since the first three equations of model (4.19) are independent of the last one, i.e., $R(x,t) = N(x,t) - S(x,t) - E(x,t) - I(x,t)$, it suffices to consider model (4.19) with three equations as follows:

$$\begin{aligned} d_1 k^2 S'' + vkS' + \Lambda - \frac{\beta SI}{1+\eta I} - \mu S &= 0, \\ d_2 k^2 E'' + vkE' + \frac{\beta SI}{1+\eta I} - (\mu+\varepsilon)E &= 0, \\ d_3 k^2 I'' + vkI' + \varepsilon E - (\mu+\lambda+\delta)I &= 0, \end{aligned} \tag{4.30}$$

The transformation $W = tanh(z)$ is used to seek the closed solutions. The travelling wave solutions are as follows:

$$\begin{aligned} S(W) &= F_1(W) = \sum_{n=0}^{N} a_n W^n, \\ E(W) &= F_2(W) = \sum_{n=0}^{N} b_n W^n, \\ I(W) &= F_3(W) = \sum_{n=0}^{N} c_n W^n, \end{aligned} \tag{4.31}$$

Substituting (4.31) into (4.30) yields;

$$\begin{aligned}
d_1k^2(1-W^2)\frac{d}{dW}\left[(1-W^2)\frac{dF_1}{dW}\right]+vk(1-W^2)\frac{dF_1}{dW}+\Lambda-\frac{\beta F_1(W)F_3(W)}{1+\eta F_3(W)}-\mu F_1(W) &= 0\\
d_2k^2(1-W^2)\frac{d}{dW}\left[(1-W^2)\frac{dF_2}{dW}\right]+vk(1-W^2)\frac{dF_2}{dW}+\frac{\beta F_1(W)F_3(W)}{1+\eta F_3(W)}-(\mu+\varepsilon)F_2(W) &= 0\\
d_3k^2(1-W^2)\frac{d}{dW}\left[(1-W^2)\frac{dF_3}{dW}\right]+vk(1-W^2)\frac{dF_3}{dW}++\varepsilon F_2(W)-(\mu+\lambda+\delta)F_3(W) &= 0
\end{aligned} \tag{4.32}$$

Now substituting $F_1(W)$ in equation (4.31) into the first equation of (4.32) and solving for $F_1(W)$ one obtains;

$$\begin{aligned}
&d_1k^2(1-W^2)\frac{d}{dW}\left[(1-W^2)\frac{d}{dW}\sum_{n=0}^{N}a_nW^n\right]+vk(1-W^2)\frac{d}{dW}\sum_{n=0}^{N}a_nW^n+\Lambda-\\
&\frac{\beta\sum_{n=0}^{N}a_nW^n\sum_{n=0}^{N}c_nW^n}{1+\eta\sum_{n=0}^{N}c_nW^n}-\mu\sum_{n=0}^{N}a_nW^n=0
\end{aligned} \tag{4.33}$$

$$\begin{aligned}
\Rightarrow\quad &d_1k^2(1-W^2)\frac{d}{dW}\left[(1-W^2)\sum_{n=0}^{N}na_nW^{n-1}\right]+vk(1-W^2)\sum_{n=0}^{N}na_nW^{n-1}+\Lambda-\\
&\frac{\beta\sum_{n=0}^{N}a_nc_nW^{2n}}{1+\eta\sum_{n=0}^{N}c_nW^n}-\mu\sum_{n=0}^{N}a_nW^n=0
\end{aligned} \tag{4.34}$$

$$\begin{aligned}
\Rightarrow\quad &d_1k^2(1-W^2)\left[\sum_{n=0}^{N}n(n-1)a_nW^{n-2}-\sum_{n=0}^{N}n(n+1)a_nW^n\right]+vk\sum_{n=0}^{N}na_nW^{n-1}-\\
&vk\sum_{n=0}^{N}na_nW^{n+1}+\Lambda-\frac{\beta\sum_{n=0}^{N}a_nc_nW^{2n}}{1+\eta\sum_{n=0}^{N}c_nW^n}-\mu\sum_{n=0}^{N}a_nW^n=0
\end{aligned} \tag{4.35}$$

$$\begin{aligned}
\Rightarrow\quad &d_1k^2\left[\sum_{n=0}^{N}n(n-1)a_nW^{n-2}-\sum_{n=0}^{N}n(n+1)a_nW^n-\sum_{n=0}^{N}n(n-1)a_nW^n+\sum_{n=0}^{N}n(n+1)a_nW^{n+2}\right]\\
+\quad &vk\sum_{n=0}^{N}na_nW^{n-1}-vk\sum_{n=0}^{N}na_nW^{n+1}+\Lambda-\frac{\beta\sum_{n=0}^{N}a_nc_nW^{2n}}{1+\eta\sum_{n=0}^{N}c_nW^n}-\mu\sum_{n=0}^{N}a_nW^n=0
\end{aligned} \tag{4.36}$$

To obtain the value of $N$, balance highest term of $W$ (linear and nonlinear terms) i.e., from the first term, $W^{N+2}$, the second term, $W^{N+1}$ , the third term, $W^{2N}$, and

the last term is $W^N$. Therefore, $2N = 2 + N$ hence $N = 2$. Since $z \to +\infty$ then $W \to +1$, we assume the travelling wave solution takes the following form;

$$F_1(W) \;=\; a_0(1-W)(1+a_1W), \tag{4.37}$$

Now substituting the second equation of (4.31) into the second equation in (4.32) yields

$$d_2k^2(1-W^2)\frac{d}{dW}\left[(1-W^2)\frac{d}{dW}\sum_{n=0}^{N}b_nW^n\right] + vk(1-W^2)\frac{d}{dW}\sum_{n=0}^{N}b_nW^n + \frac{\beta\sum_{n=0}^{N}a_nW^n\sum_{n=0}^{N}c_nW^n}{1+\eta\sum_{n=0}^{N}c_nW^n} - (\mu+\varepsilon)\sum_{n=0}^{N}b_nW^n = 0 \tag{4.38}$$

$$\Rightarrow\; d_2k^2(1-W^2)\frac{d}{dW}\left[(1-W^2)\sum_{n=0}^{N}nb_nW^{n-1}\right] + vk(1-W^2)\sum_{n=0}^{N}nb_nW^{n-1} + \frac{\beta\sum_{n=0}^{N}a_nc_nW^{2n}}{1+\eta\sum_{n=0}^{N}c_nW^n} - (\mu+\varepsilon)\sum_{n=0}^{N}b_nW^n = 0 \tag{4.39}$$

$$\Rightarrow\; d_2k^2(1-W^2)\left[\sum_{n=0}^{N}n(n-1)b_nW^{n-2} - \sum_{n=0}^{N}n(n+1)b_nW^n\right] + vk\sum_{n=0}^{N}nb_nW^{n-1} - vk\sum_{n=0}^{N}nb_nW^{n+1} + \frac{\beta\sum_{n=0}^{N}a_nc_nW^{2n}}{1+\eta\sum_{n=0}^{N}c_nW^n} - \mu\sum_{n=0}^{N}b_nW^n = 0 \tag{4.40}$$

$$\Rightarrow\; d_2k^2\left[\sum_{n=0}^{N}n(n-1)b_nW^{n-2} - \sum_{n=0}^{N}n(n+1)b_nW^n - \sum_{n=0}^{N}n(n-1)b_nW^n + \sum_{n=0}^{N}n(n+1)b_nW^{n+2}\right]$$
$$+\quad vk\sum_{n=0}^{N}nb_nW^{n-1} - vk\sum_{n=0}^{N}nb_nW^{n+1} + -\frac{\beta\sum_{n=0}^{N}a_nc_nW^{2n}}{1+\eta\sum_{n=0}^{N}c_nW^n} - (\mu+\varepsilon)\sum_{n=0}^{N}b_nW^n = 0 \tag{4.41}$$

Now, in the resulting equation, balance the highest linear and nonlinear terms of $W$, i.e., from the first term, $W^{N+2}$, the second term, $W^{N+1}$ , the third term, $W^{2N}$, and the last term is $W^N$. Then $2N = 2 + N$ where $N = 2$ and therefore, the solution take the form;

$$F_2(W) \;=\; b_0(1-W)(1+b_1W), \tag{4.42}$$

Lastly, substituting the third equation of (4.31) into the third equation of (4.32) yields;

$$\begin{aligned} & d_3k^2(1-W^2)\frac{d}{dW}\left[(1-W^2)\frac{d}{dW}\sum_{n=0}^{N}c_nW^n\right]+vk(1-W^2)\frac{d}{dW}\sum_{n=0}^{N}c_nW^n \\ + \quad & \varepsilon\sum_{n=0}^{N}b_nW^n-(\mu+\lambda+\delta)\sum_{n=0}^{N}c_nW^n=0 \end{aligned}$$

$$\begin{aligned} \Rightarrow \quad & d_3k^2(1-W^2)\frac{d}{dW}\left[(1-W^2)\sum_{n=0}^{N}nc_nW^{n-1}\right]+vk(1-W^2)\sum_{n=0}^{N}nc_nW^{n-1} \\ + \quad & \varepsilon\sum_{n=0}^{N}b_nW^n-(\mu+\lambda+\delta)\sum_{n=0}^{N}c_nW^n=0 \end{aligned}$$

$$\begin{aligned} \Rightarrow \quad & d_3k^2(1-W^2)\left[\sum_{n=0}^{N}n(n-1)c_nW^{n-2}-\sum_{n=0}^{N}n(n+1)c_nW^n\right]+vk\sum_{n=0}^{N}nc_nW^{n-1}- \\ & vk\sum_{n=0}^{N}nc_nW^{n+1}+\varepsilon\sum_{n=0}^{N}b_nW^n-(\mu+\lambda+\delta)\sum_{n=0}^{N}c_nW^n=0 \end{aligned}$$

$$\begin{aligned} \Rightarrow \quad & d_3k^2\left[\sum_{n=0}^{N}n(n-1)c_nW^{n-2}-\sum_{n=0}^{N}n(n+1)c_nW^n-\sum_{n=0}^{N}n(n-1)c_nW^n+\sum_{n=0}^{N}n(n+1)c_nW^{n+2}\right] \\ + \quad & vk\sum_{n=0}^{N}nc_nW^{n-1}-vk\sum_{n=0}^{N}nc_nW^{n+1}+\varepsilon\sum_{n=0}^{N}b_nW^n-(\mu+\lambda+\delta)\sum_{n=0}^{N}c_nW^n=0 \end{aligned} \tag{4.43}$$

To obtain the parameter $N$, balance the highest linear and nonlinear terms of highest order in the resulting equation, which yields $N=0$, implying that $c_n=0$, thus, the solution takes the form;

$$F_3(W)=c_0(1-W)(1+c_1W)=0 \tag{4.44}$$

where $c_0=0$ and $c_1=0$. Therefore, $F_3(W)=0$.

Substituting equation (4.37), (4.42), and (4.44) into equation (4.32), the following results are obtained;

$$\begin{aligned} \Rightarrow \quad & d_1k^2(1-W^2)\frac{d}{dW}\left[(1-W^2)a_0(-1+a_1(1-2W))\right]+vk\left[a_0(1-W^2)(-1+a_1(1-W))\right] \\ + \quad & \Lambda-\mu\left[a_0(1-w)(1+a_1W)\right]=0 \end{aligned}$$

$$\Rightarrow \quad d_1 a_0 k^2(1-W^2)\frac{d}{dW}\left[a_1 - 1 - 2a_1 W - a_1 W^2 + W^2 + 2a_1 W^3\right] + \tag{4.45}$$
$$vka_0\left[a_1 - 1 - 2a_1 W - a_1 W^2 + W^2 + 2a_1 W^3\right] + \Lambda - \mu a_0\left[1 + a_1 W - W - a_1 W^2\right] = 0$$

$$\Rightarrow \quad d_1 k^2 a_0\left[-2a_1 - 2a_1 W + 2W + 8a_1 W^2 + 2a_1 W^3 - 2W^3 - 6a_1 W^4\right] + \tag{4.46}$$
$$vka_0\left[a_1 - 1 - 2a_1 W - a_1 W^2 + W^2 + 2a_1 W^3\right] + \Lambda - \mu a_0\left[1 + a_1 W - W - a_1 W^2\right] = 0$$

From equation (4.46) yields the system of algebraic equations for $a_0$, $a_1$, $k$, and $v$:

$$\begin{aligned} W^3 &: \quad a_1 d_1 k - d_1 k + a_1 v = 0, \\ W^2 &: \quad 8a_1 d_1 k^2 + vk - vka_1 + \mu a_1 = 0, \\ W^1 &: \quad 2d_1 k^2 - 2d_1 k^2 a_1 - 2a_1 vk - \mu a_1 + \mu = 0, \\ W^0 &: \quad 2a_0 a_1 d_1 k^2 + a_0 a_1 vk + vka_0 - \Lambda + \mu a_0 = 0, \end{aligned} \tag{4.47}$$

Substituting equation (4.42) into (4.32) yields;

$$\Rightarrow \quad d_2 k^2(1-W^2)\frac{d}{dW}\left[(1-W^2)b_0(-1+b_1(1-2W))\right] + vk\left[b_0(1-W^2)(-1+b_1(1-W))\right]$$
$$+ \quad \Lambda - (\mu+\varepsilon)\left[b_0(1-w)(1+b_1 W)\right] = 0$$

$$\Rightarrow \quad d_2 k^2 b_0(1-W^2)\frac{d}{dW}\left[b_1 - 1 - 2b_1 W - b_1 W^2 + W^2 + 2b_1 W^3\right] + \tag{4.48}$$
$$vkb_0\left[b_1 - 1 - 2b_1 W - b_1 W^2 + W^2 + 2b_1 W^3\right] - (\mu+\varepsilon)b_0\left[1 + b_1 W - W - b_1 W^2\right] = 0$$

$$\Rightarrow \quad d_2 k^2 b_0\left[-2b_1 - 2b_1 W + 2W + 8b_1 W^2 + 2b_1 W^3 - 2W^3 - 6b_1 W^4\right] + \tag{4.49}$$
$$vkb_0\left[b_1 - 1 - 2b_1 W - b_1 W^2 + W^2 + 2b_1 W^3\right] - (\mu+\varepsilon)b_0\left[1 + b_1 W - W - b_1 W^2\right] = 0$$

From equation (4.49) yields the algebraic equation system for $b_0$, $b_1$, $k$, and $v$:

$$\begin{aligned} W^3 &: \quad b_1 d_2 k - d_2 k + b_1 v = 0, \\ W^2 &: \quad 8b_1 d_2 k^2 + vk - vkb_1 + (\mu+\varepsilon)b_1 = 0, \\ W^1 &: \quad 2d_2 k^2 - 2b_1 d_2 k^2 - 2b_1 vk - (\mu+\varepsilon)b_1 + (\mu+\varepsilon) = 0, \\ W^0 &: \quad 2b_1 d_2 k^2 - vkb_1 + vk + (\mu+\varepsilon) = 0. \end{aligned} \tag{4.50}$$

Solving the algebraic linear systems in $a_i$ and $b_i$ $i = 0, 1$ (4.47) and (4.50) with the aid of Mathematica and Matlab yields;

$$a_0 = \frac{4\Lambda}{3\mu}, \quad a_1 = 1, \quad k = \pm\frac{1}{2}\sqrt{-\frac{\mu}{2d_1}}, \quad and \quad v \geq 0, \qquad (4.51)$$
$$b_0 = 0, \quad b_1 = 0, \quad c_0 = 0$$

In view of (4.51), the travelling wave solutions are given by;

$$\begin{aligned} S(x,t) &= \frac{4\Lambda}{3\mu}(1 - tanh^2[k(x - vt)]), \quad k = \pm\frac{1}{2}\sqrt{-\frac{\mu}{2d_1}}, \quad v \geq 0 \qquad (4.52) \\ E(x,t) &= 0 \end{aligned}$$

The equations result (4.52) indicates that the COVID-19 wave of infection attacks the susceptible population with a solitary-wave front with a velocity $v \geq 0$. This means that introducing a few infectious individuals into a completely susceptible population creates a moving transition zone. This shows that COVID-19 transmission occurs when infectious individuals move from one region to another, and thus there exists a travelling wave front connecting the disease free equilibrium and the endemic equilibrium with a minimum wave speed $v^* \geq 2\sqrt{\mu d_1} > 0$ on the susceptible population.

## 4.6 Numerical Simulations and Discussion

In MATLAB$^{TM}$ software (PDE-PE) is used to illustrate the graphical simulation describing the behaviour of model solutions (4.1). The simulation parameters are obtained from the literature, while others are estimates. For simulation purposes, the initial populations are assumed to be $S(0, x) = 3000$, $E(0, x) = 2000$, $I(0, x) = 1500$, and $R(0, x) = 1000$.

Simulation analysis of the model (4.1) are presented to graphically illustrate the behaviour of the solutions of the model with varying diffusivity rates.

**Table 4.1: The Descriptive Summary of the Model Parameters**

| Parameter | Description | Unit/value units | Source |
|---|---|---|---|
| $\Lambda$ | Recruitment rate | $3.178\times10^{-5}$ day$^{-1}$ | [39] |
| $\mu$ | Natural mortality rate | $3.91\times 10^{-5}$day$^{-1}$ | [39] |
| $\delta$ | Disease mortality rate | $1.03\times 10^{-6}$day$^{-1}$ | [6, 39] |
| $\lambda$ | Human recovery rate | 0.125 day$^{-1}$ | [5] |
| $\beta$ | Transmission coefficient | 0.02 day$^{-1}$ | Estimated |
| $\varepsilon$ | Transition rate from E to I | 0.0877 day$^{-1}$ | [10] |
| $\eta$ | Human saturation constant | 0.05 | Estimated |
| $d_1$ | Susceptible diffusivity constant | (0 - 1.0) km day$^{-1}$ | Variable |
| $d_2$ | Exposed diffusivity constant | (0 - 1.0) km day$^{-1}$ | Variable |
| $d_3$ | Infected diffusivity constant | (0 - 1.0) km day$^{-1}$ | Variable |
| $d_4$ | Recovered diffusivity constant | (0 - 1.0) km day$^{-1}$ | Variable |

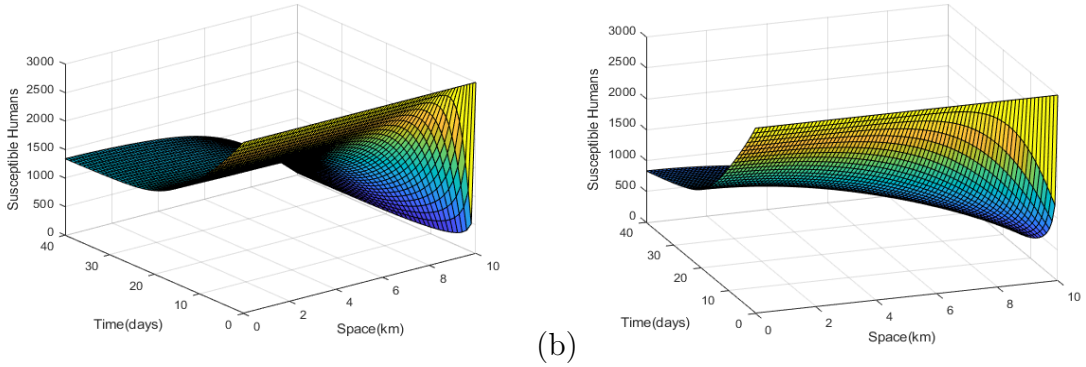


(a) (b)

**Figure 4.1: Plots (a) and (b) show the simulations of the susceptible humans corresponding to the rate of diffusion, (a) $d_1 = 0.1$ day$^{-1}$, (b) $d_1 = 0.9$ day$^{-1}$**

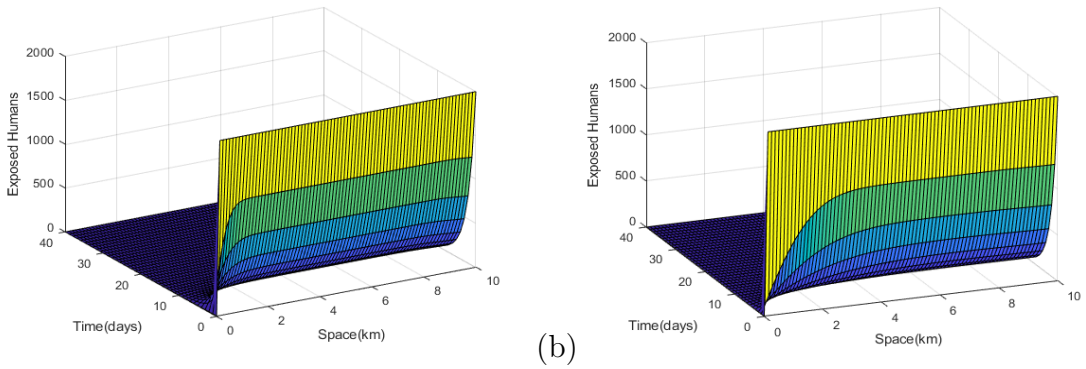


(a) (b)

**Figure 4.2: Plots (a) and (b) show the simulations of the exposed humans corresponding to the rate of diffusion, (a) $d_2 = 0.1$ day$^{-1}$, (b) $d_2 = 0.9$ day$^{-1}$**

Figure 4.1 plots (a) and (b) show simulations of susceptible humans for varying diffusivity rate values, $d_1$ at 0.1 and 0.9 respectively. The number of the suscep-

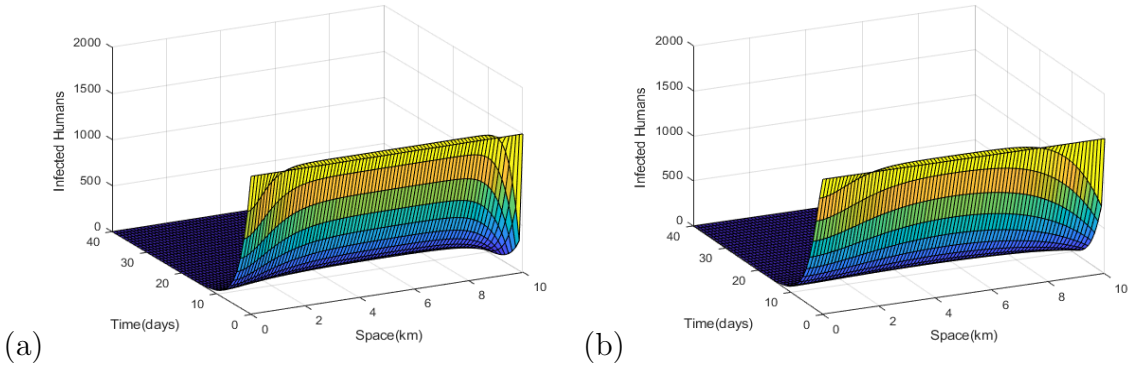


**Figure 4.3: Plots (a) and (b) show the simulations of the infected humans corresponding to the rate of diffusion, (a) $d_3 = 0.1$ day$^{-1}$, (b) $d_3 = 0.9$ day$^{-1}$**

tible humans reduces faster when diffusivity rate is high and also reduces with an increase in space. When $d_1 = 0.9$, it would take less days for a pool of susceptible humans to be exposed to the virus. When diffusivity rate is low, $d_1 = 0.1$, there is a slow increase of exposed individuals.

Figure 4.2 plots (a) and (b) show simulations of exposed humans for varying diffusivity rate values, $d_2$ at 0.1 and 0.9 respectively. They show that the number of the exposed humans increases faster when diffusivity rate is high and also increases with space. Figure 4.3 plots (a) and (b) show the spatiotemporal simulations of infected humans for varying diffusivity rate values of $d_3$. They show that as rate of diffusion (human mobility), $d_3$ increases the number of infected individuals increases. This means that, human mobility has an effected in the transmission dynamics of COVID-19. Infectious individuals will spread to regions where there is no infection until an equilibrium is reached. The numerical result demonstrates that the movement of infectious individuals causes the disease to persist in the population. This results in the formation of a wave profile, implying that the introduction of an infective individual into a susceptible population results in infection propagation.

From the study findings, COVID-19 persists in the population if there exists movement of infected individuals. The introduction of an infected individual into a purely susceptible population would cause "a propagating wave" of infection in the population. Therefore, a travelling wave profile exists that connects the disease-free equilibrium and the endemic equilibrium. The results in this study are in agreement with the study done in [40, 59]. The Tanh method was successfully applied to establish exact solutions of the model. The result revealed that COVID-19 wave of infection attacks the susceptible population with a solitary-wave front with a velocity $v \geq 0$. Provided that $v^* > 0$ is the minimum speed required to cause an infection in the susceptible population. From the numerical simulations, it is shown that human mobility play crucial role for disease transmission. Therefore, control interventions such as, lockdown, travel restrictions, cessation of movement e.t.c., that would reduce human mobility may play a major role in reducing the spread of COVID-19. These interventions targets at creating barriers to curtail the spread of the virus in the affected regions.

# CHAPTER FIVE

# DYNAMICS OF COVID-19 MODEL WITH VACCINATION

## 5.1 Introduction

In modern medicine, vaccination has been an important public health technique for reducing the burden of many human infectious diseases [43, 44, 52]. COVID-19 vaccines such as Pfizer, Morderna, AstraZeneca, Sputnik, Sinopharm, Johnson & Johnson, and others are currently being administered around the world. Due to a shortage of COVID-19 vaccines in many developing countries, different vaccination strategies have been implemented, with varying results. Ring and targeted vaccination techniques are among them [4]. For example in Kenya prioritization is given to adult population (Due to their low immunity level) [48]. COVID-19 dynamics model with vaccination as an intervention is proposed in this study.

## 5.2 Model Formulation

To assess the impact of vaccination as a control intervention, a compartment of vaccinated individuals is introduced into the model (3.1). It is assumed that the vulnerable population will be vaccinated at a rate $\gamma$, where $(0 < \gamma \leq 1)$. When vaccinated individuals are exposed to the virus, they may contract the virus depending on the type of vaccine efficacy level administered to an individual. Thus, the probability of vaccinees contracting an infection is given by $\beta_1 := (1 - \vartheta)\beta$, where $\beta$ is the probability of virus transmission of the susceptible individual upon interaction with an infectious individual. The vaccine efficacy parameter $\vartheta$ is defined as $(0 < \vartheta \leq 1)$. Since the vaccinee is assumed to have acquired vaccine-induced immunity, the probability of transmission $(\beta_1)$ is assumed to be lower than $\beta$ [30, 39]. The natural mortality rate in the human population is assumed to be $\mu$.

The above model description translates into the following schematic flow diagram.

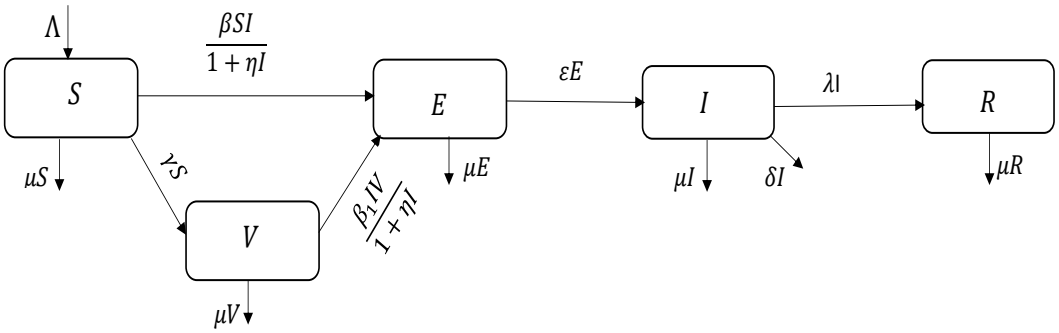


**Figure 5.1: A Schematic Flow Diagram of COVID-19 Dynamics Model with Vaccination**

From the description above, the model is represented by the following set of ordinary differential equations (odes)

$$\begin{aligned}
\frac{dS}{dt} &= \Lambda - \frac{\beta SI}{1+\eta I} - (\mu+\gamma)S, \\
\frac{dV}{dt} &= \gamma S - \frac{\beta_1 V I}{1+\eta I} - \mu V, \\
\frac{dE}{dt} &= \frac{(\beta S + \beta_1 V)I}{1+\eta I} - (\mu+\varepsilon)E, \\
\frac{dI}{dt} &= \varepsilon E - (\mu+\lambda+\delta)I, \\
\frac{dR}{dt} &= \lambda I - \mu R.
\end{aligned} \tag{5.1}$$

where; $\beta_1 < \beta$, $\quad S = S(t),\ \ V = V(t),\ \ E = E(t),\ \ I = I(t),\ \ R = R(t),$

$$\{S, V, E, I, R\} \in \mathbb{R}^5_+$$

## 5.3 Well-posedness of the model

Since the model (5.1) describes the human population, all state variables will remain positive, so solutions of the model (5.1) with positive initial conditions will remain positive and non-negative for all $t \geq 0$.

## 5.4 The Vaccine Reproduction Number and the Disease Free Equilibrium

In this section the vaccine reproductive number $R_V$ and the disease-free equilibrium of model (5.1) are computed.

### 5.4.1 The Disease-free equilibrium

The disease-free equilibrium (DFE) point of model (5.1) is defined as the absence of infection in the population under study.

**Proposition 5.4.1.** *There exists a DFE of model (5.1) given by*

$$E_0 = (S^0, V^0, E^0, I^0, R^0) = \{\frac{\Lambda}{\mu+\gamma}, \frac{\gamma\Lambda}{\mu(\mu+\gamma)}, 0, 0, 0\}.$$

*Proof.* From the first and second equations of model (5.1) where $S \neq 0$, $V \neq 0$, and $E = I = R = 0$, then $S^0 = \frac{\Lambda}{\mu+\gamma}$ and $V^0 = \frac{\gamma\Lambda}{\mu(\mu+\gamma)}$. Therefore, model (5.1) has a disease free equilibrium given by

$$E_0 = \left[\frac{\Lambda}{\mu+\gamma}, \frac{\gamma\Lambda}{\mu(\mu+\gamma)}, 0, 0, 0\right].$$

□

### 5.4.2 Vaccine Reproduction Number $R_V$

The vaccine reproduction number, $R_V$, is a threshold quantity that can predict the spread of a disease in a given population in the presence of an intervention, e.g, vaccination. The vaccine reproduction number is given by $R_V = \rho(FV^{-1})$, where $(FV^{-1})$ is the spectral radius of the next generation matrix $(FV^{-1})$ as computed in section 3.4.1. Therefore,

$$\begin{aligned} R_V &= \frac{\Lambda\varepsilon\beta(\mu+(1-\vartheta)\gamma)}{\mu(\mu+\varepsilon)(\mu+\lambda+\delta)(\mu+\gamma)}, \\ &= \frac{\Lambda\varepsilon\beta}{\mu(\mu+\varepsilon)(\mu+\lambda+\delta)}.\frac{(\mu+(1-\vartheta)\gamma)}{(\mu+\gamma)}, \\ &= R_0\left[\frac{\mu+(1-\vartheta)\gamma}{\mu+\gamma}\right]. \end{aligned} \tag{5.2}$$

where the basic reproduction number $R_0$ is computed in equation (4.13).

The vaccine reproduction number $R_V$ is a measure of the severity of an epidemic and one of the most important parameters, as it determines whether or not the disease will infiltrate a population. This means that if $R_V < 1$, the infection dies out, whereas if $R_V > 1$, the disease persists in the population and may cause an epidemic.

## 5.5 The Effect of Vaccination Rate and Vaccine Efficacy on the COVID-19 Epidemic

In this section, the proportion/fraction of the population to be vaccinated so as to reach a herd immunity is investigated. Consider the vaccine reproduction number $R_V$ of the model (5.1) given by

$$\begin{aligned} R_V &= \frac{\Lambda\varepsilon\beta(\mu + (1-\vartheta)\gamma)}{\mu(\mu+\varepsilon)(\mu+\lambda+\delta)(\mu+\gamma)}, \\ &= R_0\left[\frac{\mu + (1-\vartheta)\gamma}{\mu+\gamma}\right]. \end{aligned} \tag{5.3}$$

Now taking $R_V < 1$, since in the presence of interventions such as vaccination $R_V$ will be less than unity.

$$R_V = R_0\left[\frac{\mu + (1-\vartheta)\gamma}{\mu+\gamma}\right] < 1, \tag{5.4}$$

then

$$R_0\left[\frac{\mu + (1-\vartheta)\gamma}{\mu+\gamma}\right] < 1, \tag{5.5}$$

Making the rate of vaccination $\gamma$ the subject in equation (5.5), one obtains

$$\gamma > \frac{\mu[R_0 - 1]}{[1 - R_0(1-\vartheta)]}. \tag{5.6}$$

From equation (5.6), in the presence of an infection i.e., for a fixed $R_0 > 1$ $[3.49 - 4.11]$[32]. Taking $R_0 = 4.11$, it is clear that when the efficacy of a certain vaccine is low, say at 76%, $\vartheta = 0.76$, the rate of vaccination $\gamma$ would be

higher. This means that there would be need to vaccinate high proportion of individuals so as to reach a herd immunity. On the other hand, when a vaccine efficacy is high, say 90%, $\vartheta = 0.9$, the rate of vaccination, $\gamma$, would be lower. This means that a small population need to be vaccinated so as to reach a herd immunity.

Furthermore, from equation (5.3);

$$R_V = R_0 \left[ \frac{\mu + (1 - \vartheta)\gamma}{\mu + \gamma} \right].$$

when the vaccination rate $\gamma = 0$ or $\vartheta = 0$, then $R_V = R_0$. As the vaccination rate increases, with a constant vaccine efficacy, then $R_V$ will be reducing with time. On the other hand, with rate of vaccination held at a constant, as the efficacy of a certain vaccine increases then $R_V$ will also be reducing with time. Thus, the values of the rate of vaccination and the vaccine efficacy can be used to determine the intensity of control measures that need to be implemented in order to contain the COVID-19 epidemic.

Kenya's government had planned to vaccinate about $27,246,033$ which is approximately 50% of its population by end of June 2022 in a phased approach [48]. As of June $4^{th}$, 2022, Kenya had administered a total of $18,271,847$ vaccines across the country. Only $8,462,289$ people were fully vaccinated, accounting for 31.1% of the target population [46]. Herd immunity, also known as community immunity, occurs when a large proportion of a region's or country's population is immune to a specific disease. This means that the individuals are immune to the disease, preventing an occurrence of epidemic. Herd immunity against COVID-19 in Kenya should be achieved by immunizing a significant proportion of its citizens [24, 46].

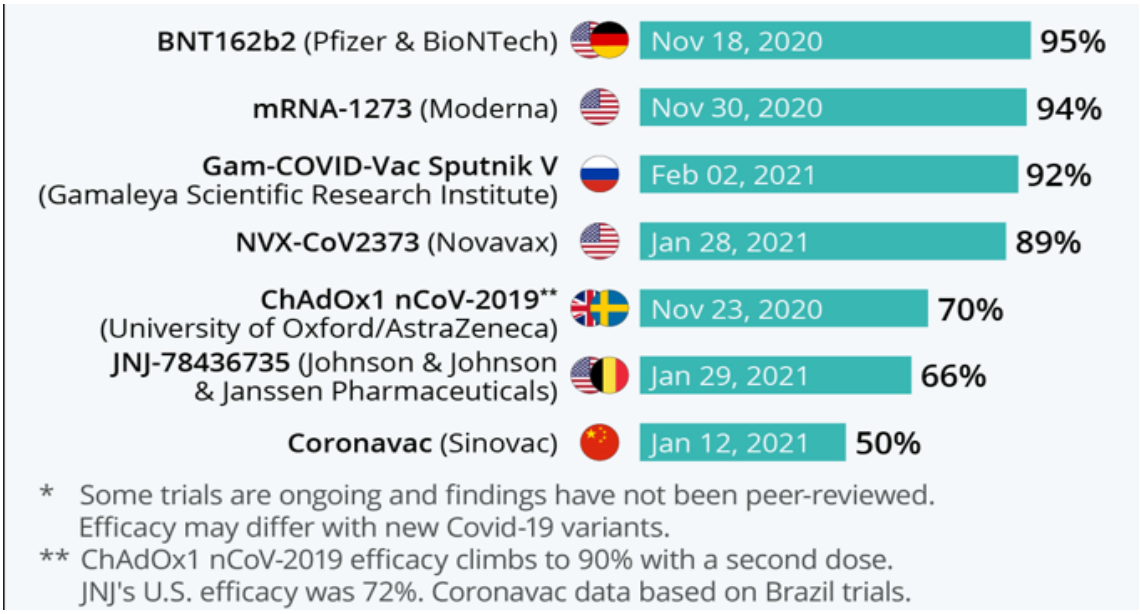


**Figure 5.2: Estimated Vaccine Effectiveness of COVID-19 Prevention Based on Interim Data from Late-stage Clinical Trials**
**Source: Respective Companies, The Lancet, Butantan Institute, Feb, 2021**

Figure 5.2 show the estimated effectiveness of COVID-19 vaccines based on interim data from late-stage clinical trials done between November 2020 and January 2021. BNT162b2(Pfizer and BioNTech) have the highest effectiveness with 95% and the lowest is Coronavac(Sinovac) with 50% effectiveness.

### 5.6 Sensitivity Analysis

The degree to which an input parameter influences a model's output is known as sensitivity. Sensitivity analysis of the vaccine reproduction number can be used to develop a mitigation strategy that will slow the spread of the pandemic by lowering $R_V$, [23]. Sensitive parameters are those that have a significant impact on an infection's transmission dynamics. The normalised forward sensitivity index, [21], the sensitivity indices of the model as shown in section 3.6 with an vaccine reproduction number of model (5.1) given in equation (5.3);

$$R_V = \frac{\Lambda\varepsilon\beta(\mu+(1-\vartheta)\gamma)}{\mu(\mu+\varepsilon)(\mu+\lambda+\delta)(\mu+\gamma)},$$

$$R_V = R_0\left[\frac{\mu+(1-\vartheta)\gamma}{\mu+\gamma}\right]. \tag{5.7}$$

The sensitivity indices are as computed below;

$$\begin{aligned}
\Upsilon_{\Lambda}^{R_V} &= \frac{\partial R_V}{\partial \Lambda}\times\frac{\Lambda}{R_V}=1,\\
\Upsilon_{\beta}^{R_V} &= \frac{\partial R_V}{\partial \beta}\times\frac{\beta}{R_V}=1,\\
\Upsilon_{\gamma}^{R_V} &= \frac{\partial R_V}{\partial \gamma}\times\frac{\gamma}{R_V}=\frac{(1-\vartheta)\gamma}{\mu+(1-\vartheta)\gamma}-\frac{\gamma}{\mu+\gamma},\\
\Upsilon_{\vartheta}^{R_V} &= \frac{\partial R_V}{\partial \vartheta}\times\frac{\vartheta}{R_V}=-\frac{\vartheta\gamma}{\mu+(1-\vartheta)\gamma}.
\end{aligned}$$

In a similar manner all other parameters can be computed.

Table 5.1 gives a summary of the $R_V$ sensitivity indices evaluated at the baseline parameter values given in Table 5.2.

**Table 5.1: Sensitivity Indices of $R_V$ with Respect to the Model Parameters.**

| Parameter | Description | Sensitivity index |
|---|---|---|
| $\Lambda$ | Recruitment rate | 1 |
| $\beta$ | Transmission Coefficient | 1 |
| $\varepsilon$ | Transition rate from E to I | -0.999843 |
| $\mu$ | Natural death rate | $7.81816576\times10^{-5}$ |
| $\gamma$ | Rate of vaccination | -0.8984463 |
| $\vartheta$ | Vaccine efficacy | -0.9998436 |
| $\lambda$ | Recovery rate | -0.999679 |
| $\delta$ | Disease mortality rate | -0.000008237 |

From the sensitivity analysis as presented in Table 5.1, an increase of the rate of vaccination $\gamma$ by 1% leads to a decrease of the effective reproduction $R_V$ by 0.89844626%. An increase of the vaccine efficacy $\vartheta$ by 1%, leads to a decrease of the vaccine reproductive number $R_V$ by 0.9990436%. From the sensitivity indices in Table 5.1, the rate of vaccination and the vaccine efficacy are among the sensitive parameters of $R_V$. An increase in the rate of vaccination with a high vaccine

efficacy, leads to a decrease in the vaccine reproduction number. Consequently control strategies should target an increased rate of vaccination and administration vaccines of high efficacy levels.

### 5.7 Optimal Analysis with Vaccination as a Preventive Strategy

An optimal control problem is constructed to effectively control COVID-19 virus spread and optimizing the vaccination program. From the sensitivity analysis in section 5.6 above, it is shown that the rate of vaccination $\gamma$ and the vaccine efficacy $\vartheta$ are among the most sensitive parameters of the vaccine reproduction number $R_V$. Therefore in this section, optimal control is performed to understand the effects of these parameter on optimum vaccination program. To determine the optimum vaccination program of COVID-19, let the variables $\gamma^*$ and $\beta_1^* =: (1-\vartheta)\beta$ be the control variables. As a result, an optimum control problem is constructed, with the goal of reducing the number of individuals infected with COVID-19. To accomplish this, the following objective function is developed:

$$J = \int_0^\tau [P_0 S + P_1 V + P_2 E + P_3 \gamma^2 + P_4 \beta_1^2] dt, \tag{5.8}$$

where $[0, \tau]$ is the entire time horizon over the control applied and $P_0$, $P_1$, $P_2$, $P_3$, $P_4$ are positive weights that balance the relative importance of terms in the objective functional $J$. An optimal control $\gamma^*$, $\beta_1^*$ is chosen as;

$$J(\gamma^*, \beta_1^*) = min\{J(\gamma, \beta_1)\}, \tag{5.9}$$

such that $(\gamma, \beta_1)$ are measurable with $0 \leq \gamma \leq \beta_1 \leq 1$. This necessary condition that optimal control must satisfy, from the Pontryagin's Maximum Principle [49]. The Hamilitonian function is;

$$\begin{aligned} H &= P_0 S + P_1 V + P_2 E + P_3 \gamma^2 + P_4 \beta_1^2 + \Phi_s[\Lambda - \frac{\beta S I}{1+\eta I} - (\mu+\gamma)S] + \\ &\quad \Phi_V[\gamma S - \frac{\beta_1 V I}{1+\eta I} - \mu V] + \Phi_E[\frac{(\beta S + \beta_1 V) I}{1+\eta I} - (\mu+\varepsilon)E] \\ &\quad + \Phi_I[\varepsilon E - (\mu+\lambda+\delta)I] + \Phi_R[\lambda I - \mu R]. \end{aligned}$$

where $\Phi_S$, $\Phi_V$, $\Phi_E$, $\Phi_I$, and $\Phi_R$ are the adjoint variables. Using the Pontryagin's maximum principle and the existence for optimal control [49, 50] to obtain the expression of optimal controls in order to minimize the number of infections in the population and the cost of control strategies. The following proposition is applied

**Proposition 5.7.1.** *For the optimal control $(\gamma, \beta_1)$ that minimizes $J(\gamma, \beta_1)$, the adjoint variables $\Phi_S$, $\Phi_V$, $\Phi_E$, $\Phi_I$, and $\Phi_R$ satisfy the following ordinary differential equations*

$$\begin{aligned}
\frac{d\Phi_S}{dt} &= P_0 - \Phi_S\frac{\beta I}{1+\eta I} - (\mu+\gamma)\Phi_S + \gamma\Phi_V + \Phi_E\frac{\beta I}{1+\eta I},\\
\frac{d\Phi_V}{dt} &= P_1 - \Phi_V\frac{\beta I}{1+\eta I} - \mu\Phi_V + \Phi_E\frac{\beta_1 I}{1+\eta I},\\
\frac{d\Phi_E}{dt} &= P_2 - (\mu+\varepsilon)\Phi_E + \varepsilon\Phi_I,\\
\frac{d\Phi_I}{dt} &= -\Phi_S\frac{\beta S}{(1+\eta I)^2} - \Phi_V\frac{\beta_1 V}{(1+\eta I)^2} + \Phi_E\frac{(\beta S+\beta_1 V)}{(1+\eta I)^2} - \Phi_I(\mu+\lambda+\delta) + \lambda\Phi_R,\\
\frac{d\Phi_R}{dt} &= \mu\Phi_R.
\end{aligned} \tag{5.10}$$

*with tranversality conditions*

$$\Phi_S(\tau) = \Phi_V(\tau) = \Phi_E(\tau) = \Phi_I(\tau) = \Phi_R(\tau) = 0,$$

*thus the optimal control takes the characterization form*

$$\gamma^* = \max\left[0, min\left(1, \frac{S(\Phi_S - \Phi_V)}{2P_3}\right)\right] \tag{5.11}$$

$$\beta_1^* = \max\left[0, min\left(1, \frac{VI(\Phi_V - \Phi_E)}{2(1+\eta I)P_4}\right)\right] \tag{5.12}$$

*Proof.* The Hamilitonian $H$ in equation (5.10) is differentiated with respect to the state variables, $S, V, E, I, R$ respectively. Thus, the adjoint of the system can be written as;

$$\Phi_M = -\frac{\partial H}{\partial M},$$

for

$$M = \{S, V, E, I, R\},$$

By the Pontryagin's Maximum Principle [49, 50], $H$ can be maximized with respect to $\gamma$ and $\beta_1$, that is;

$$\begin{aligned} 0 = \frac{\partial H}{\partial \gamma}|_{\gamma^*} &= 2P_3\gamma - \Phi_S S - \Phi_V S, \\ \Rightarrow \gamma^* &= \frac{S(\Phi_S - \Phi_V)}{2P_3}. \end{aligned}$$

$$\begin{aligned} 0 = \frac{\partial H}{\partial \beta_1}|_{\beta_1^*} &= 2P_4\beta_1 - \Phi_V \frac{VI}{1+\eta I} + \Phi_E \frac{VI}{1+\eta I}, \\ \Rightarrow \beta_1^* &= \frac{VI(\Phi_V - \Phi_E)}{2(1+\eta I)P_4}. \end{aligned}$$

Taking the bounds on $\gamma$ and $\beta_1$ into account, the characterization of $\gamma^*$ and $\beta_1^*$ is obtained as shown in equations (5.11) and (5.12) respectively. Now using the control arguments $0 \leq \gamma \leq \beta_1 \leq 1$, then;

$$\gamma^* = \begin{cases} 0 & \text{if} \quad \xi_1^* \leq 0 \\ \xi_1^* & \text{if} \quad 0 < \xi_1^* < 1 \\ 1 & \text{if} \quad \xi_1^* \geq 1 \end{cases} \tag{5.13}$$

$$\beta_1^* = \begin{cases} 0 & \text{if} \quad \xi_2^* \leq 0 \\ \xi_2^* & \text{if} \quad 0 < \xi_2^* < 1 \\ 1 & \text{if} \quad \xi_2^* \geq 1 \end{cases} \tag{5.14}$$

where

$$\xi_1^* = \frac{S(\Phi_S - \Phi_V)}{2P_3}.$$

$$\xi_2^* = \frac{VI(\Phi_V - \Phi_E)}{2(1+\eta I)P_4}.$$

□

Since the optimal control switches at most once, then the control objective function constructed in this study must have been optimal.

In recent decades, control theory has been widely applied in many fields. Optimal control, particularly in epidemiology, could be very useful in controlling mathematical models depicting the spread of infectious diseases [9]. The appropriate

regulation of disease dynamics is specified in the form of restrictions, according to the biological interpretation of the objective functional. The control's objectives must be met exclusively within these limits. Furthermore, lowering illness prevalence requires reducing the total number of infectious cases. This entails increasing the rate of vaccination ($\gamma$) while decreasing the coefficient of contracting the infection $\beta_1 = (1 - \vartheta)\beta$. Increased vaccination rates, administering of high efficacious vaccine would help maximize control strategies against COVID-19 transmission dynamics.

### 5.8 Numerical Simulation and Discussion

The parameters used for simulation are obtained from literature and others are estimate (cf. Table 5.2). These parameter values are varied within realistic limits. To simulate model (5.1) the following parameter are used;

**Table 5.2: The Descriptive Summary of the Model Parameters.**

| Parameter | Description | Unit/value units | Source |
|---|---|---|---|
| $\Lambda$ | Recruitment rate | $3.178\times10^{-5}$ day$^{-1}$ | [39] |
| $\mu$ | Natural mortality rate | $3.91\times 10^{-5}$day$^{-1}$ | [7] |
| $\delta$ | Disease mortality rate | $0.103\times 10^{-5}$day$^{-1}$ | [6, 39] |
| $\beta$ | Transmission probability | 0.02 day$^{-1}$ | Estimated |
| $\beta_1$ | Vaccinee transmission probability | 0.05 day$^{-1}$ | Estimated |
| $\vartheta$ | Vaccine efficacy | (0 - 1.0) | Variable |
| $\gamma$ | Rate of vaccination | (0 - 1.0) | Variable |
| $\varepsilon$ | Transition rate from E to I | 0.5 day$^{-1}$ | Estimated |
| $\eta$ | Human saturation constant | 0.05 | Estimated |
| $\lambda$ | Human recovery rate | 0.125 day$^{-1}$ | [25] |

For purposes of simulation, unless otherwise stated, the initial populations are assumed to be $S(0) = 3000$, $V(0) = 2000$, $E(0) = 1500$, $I(0) = 1200$, and $R(0) = 1000$. The numerical simulation aims to analyze the change in state of COVID-19 virus progression over time, as well as the impact of variation in vaccination rate and vaccine efficacy on COVID-19 transmission dynamics. This is accomplished

by varying the parameters $\vartheta$ and $\gamma$ while holding the other parameters constant. Simulation analysis of the model (5.1) are presented.

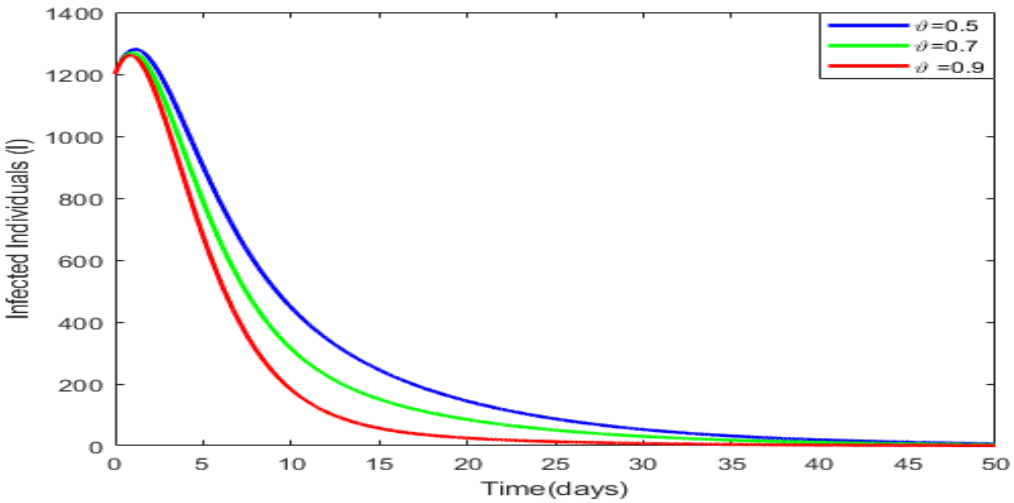


**Figure 5.3: The effect of variation in vaccine efficacy ($\vartheta$) on infection dynamics**

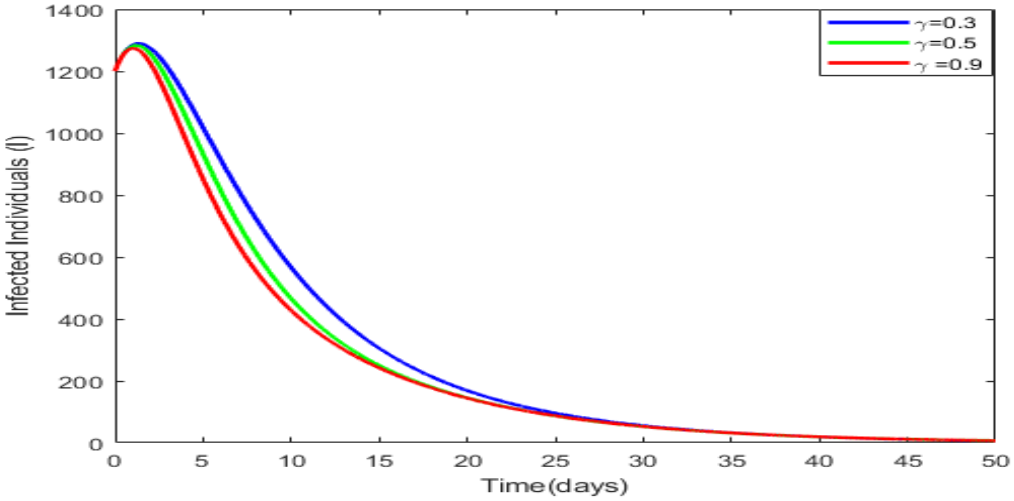


**Figure 5.4: The effect of variation in vaccination rate ($\gamma$) on infection dynamics**

Figure 5.3 show the graph of infected individuals against time with varying vaccine efficacy $\vartheta$. In the presence of a constant rate of vaccination at 50%, it would take less time for a pool of infected individual to reduce when the vaccine administered is of high efficacy, say 90% efficacy as depicted in the graph. On the other hand when the vaccine efficacy is low, it would take longer time for the infected individuals reduce, therefore COVID-19 infection would persist in the population.

Figure 5.4 show the graph infected individuals with a varying rate of vaccination with vaccine efficacy of 90%. It is observed that when the rate of vaccination ($\gamma = 0.90$), the number of infected individuals decrease sharply within the first few days and when the rate of vaccination is very low ($\gamma = 0.30$) the number of infected individuals are reducing at slower rate.

Given the emergence of highly transmissible new variants, decreased vaccine effectiveness, and unequal vaccine availability, there is growing concern that vaccination may fail to produce herd immunity [48]. Vaccination offers a very powerful method of COVID-19 disease control [30, 36, 39]. The result show that the critical level of vaccination so as to reach a herd immunity would be approximately 50% and above with an efficacy rate $> 80\%$ is required to eradicate the infection from the population. Some vaccines currently on offer have very low efficacy and therefore having a disadvantageous effects.

# CHAPTER SIX

# CONCLUSIONS AND RECOMMENDATIONS

## 6.1 Introduction

In this chapter, conclusions and recommendations are drawn from the study.

## 6.2 Conclusions

In this study, COVID-19 transmission dynamics mathematical model with interventions is developed and analysed. The dynamics of COVID-19 with varying transmission rate is developed and analysed in the first model. The bifurcation analysis show that the varying transmission rate plays a major role on the COVID-19 transmission dynamics. It is clear from the numerical simulations that reducing the transmission coefficient would curtail the spreading of the infection. This may be achieved by reducing the interaction between infectious humans and susceptible population through measures such as cessation of movements and social distancing.

In the second model, a diffusive COVID-19 dynamics model with constant transmission coefficient is developed and analysed in order to focus solely on the effect of diffusion (human mobility). When infected individuals are introduced into a fully susceptible population, the model analysis reveals that a moving transition from the disease free equilibrium to the endemic equilibrium occurs. The Tanh Method is used to compute the exact solutions of the travelling wave front. From the numerical analysis it is shown that human mobility play a crucial role in the disease transmission. Therefore, interventions that have an effect on diffusion, such as lockdown, travel restrictions, and cessation of movement, among others, may be important in controlling and preventing the spread of COVID-19.

Finally, a model incorporating vaccination is developed and analysed. The sensitivity analysis indicates that the rate of vaccination, $\gamma$, and the vaccine efficacy $\vartheta$ are among the most influential parameter of $R_V$. An increase in the rate of vaccination with highly efficacy vaccine reduces the vaccine reproduction number. Control strategies should therefore target these parameters. From optimal control, increasing vaccination rates and administering highly effective vaccines would help maximise control strategies against COVID-19 transmission dynamics. Based on numerical simulations of the effect of vaccination on the transmission dynamics of COVID-19, control strategies should aim to increase vaccination rates with a high efficacy vaccine. The model analysis suggests that an effective vaccination program will aid in the control of COVID-19 disease spread. This study showed that an effective vaccination program may possibly eliminate the infection in the population.

### 6.3 Recommendations

The risk assessment and management of COVID-19 infection has sparked worldwide interest. The following recommendations and possible extensions of the work are made based on the results obtained;

- It would be desirable to investigate the nature of travelling wave stability and the spatial spread in higher-dimensional space.
- Many countries are having stocks of vaccines which are nearly expiring and a large population is yet to be vaccinated. Research into the effects of vaccine hesitancy on COVID-19 transmission dynamics may be conducted.
- Future research could focus on an age-dependent SVEIR model to determine the suitable vaccination strategies to be applied with respect to age.

## REFERENCES


[1] Abdullahi, I., Baba, B. A., & Nasidi, B., (2021). Optimal control model for the transmission of novel COVID-19. *Computers, Materials, & Continua*,**(66)**, 3089–3106.

[2] Adhikari, S.P., Meng, S., Wu, Y.J., Mao, Y.P., Ye, R.X., Wang, Q.Z., Sun, C., Sylvia, S., Rozelle, S., Raat, H., & Zhou, H., (2020). Epidemiology, causes, clinical manifestation and diagnosis, prevention and control of coronavirus disease (COVID-19) during the early outbreak period: a scoping review. *Infectious diseases of poverty*, **9(1)**, 1–12.

[3] Ahmed, N., Fatima, M., Baleanu, D., Nisar, K.S., Khan, I., Rafiq, M., Rehman, M.A.U., & Ahmad, M.O., (2020). Numerical analysis of the susceptible exposed infected quarantined and vaccinated (SEIQV) reaction-diffusion epidemic model. *Frontiers in Physics*, **7**, 220.

[4] Albani, V., Loria, J., Massad, E., & Zubelli, J. P. (2021). The Impact of COVID-19 Vaccination Delay: A Modelling Study for Chicago and NYC Data. *arXiv preprint arXiv:2102.12299*.

[5] Aleta, A., Martin-Corral, D., Pastore y Piontti, A., Ajelli, M., Litvinova, M., Chinazzi, M., Dean, N.E., Halloran, M.E., Longini Jr, I.M., Merler, S., & Pentland, A., (2020). Modelling the impact of testing, contact tracing and household quarantine on second waves of COVID-19. *Nat Hum Behav*, **4(9)**, 964-971.

[6] Anderson, R. M. & May, R. M., (1991), *Infectious Disease of Human: Dynamics and Control*, London, Oxford University Press.

[7] Amaku, M., Covas, D. T., Coutinho, F. A. B., Azevedo, R. S., & Massad, E. (2021). Modelling the impact of delaying vaccination against SARS-CoV-2 assuming unlimited vaccine supply. *Theoretical Biology and Medical Modelling*, **18(1)**, 1–11.

[8] Apima, S. B., & Mutwiwa, J. M. (2020). An SEIQR Mathematical Model for The Spread of COVID-19. *Journal of Advances in Mathematics and Computer Science*, **35(6)**, 35–41.

[9] Araz, S. $\dot{I}$. (2021). Analysis of a Covid-19 model: optimal control, stability and simulations. *Alexandria Engineering Journal*, **60(1)**, 647-658.

[10] Asamoah, J. K. K., Bornaa, C. S., Seidu, B., & Jin, Z. (2020). Mathematical analysis of the effects of controls on transmission dynamics of SARS-CoV-2. *Alexandria Engineering Journal*, **59(6)**, 5069–5078.

[11] Azevedo, L., Pereira, M. J., Ribeiro, M., & Soares, A. (2020). Spatiotemporal modelling of COVID-19 infection risk in Portugal, *Research Square*.

[12] Baba, I. A., Nasidi, B. A., & Baleanu, D. (2021). Optimal control model for the transmission of novel COVID-19, *Computers, Materials and Continua*, **66(3)**, 3089 –3106

[13] Beer, G., & Garrido, M. I. (2015). Locally Lipschitz functions, cofinal completeness, and UC spaces. *Journal of Mathematical Analysis and Applications*, **428(2)**, 804–816.

[14] Bubar, K. M., Reinholt, K., Kissler, S. M., Lipsitch, M., Cobey, S., Grad, Y. H., & Larremore, D. B. (2021). Model-informed COVID-19 vaccine prioritization strategies by age and serostatus. *Science*, **371(6532)**, 916–921.

[15] Capasso, V., & Serio, G. (1978). A generalization of the Kermack-McKendrick deterministic epidemic model. *Mathematical biosciences*, **42(1-2)**, 43–61.

[16] Castillo,C. C, & Song, B.(2004). Dynamical models of tuberculosis and their applications. *Mathematical Biosciences and Engineering*. **1(2)**, 361-404.

[17] Cevik, M., Kuppalli, K., Kindrachuk, J., & Peiris, M. (2020). Virology, transmission, and pathogenesis of SARS-CoV-2. *bmj*, 371.

[18] Cevik, M., Bamford, C., & Ho, A. (2020). COVID-19 pandemic a focused review for clinicians. *Clinical Microbiology and Infection*, **26(7)**, 842–847.

[19] Cevik, M., Marcus, J., Buckee, C., & Smith, T. (2021). SARS-CoV-2 transmission dynamics should inform policy. *Clinical Infectious Diseases*, **73(Supplement$_2$)**, S170–S176.

[20] Chen, Y. C., Lu, P. E., Chang, C. S., & Liu, T. H. (2020). A time-dependent SIR model for COVID-19 with undetectable infected persons. *IEEE Transactions on Network Science and Engineering*, **7(4)**, 3279–3294.

[21] Chitnis N., Hyman J. M., & Cushing J. M., (2008). Determining Important parameters in the spread of malaria through sensitivity analysis of a mathematical model. *Bull Math Biol.* **70(5)**, 1272–1296.

[22] Chitnis, N., Cushing, J. M., & Hyman, J. M. (2006). Bifurcation analysis of a mathematical model for malaria transmission. *SIAM Journal on Applied Mathematics*, **67(1)**, 24–45.

[23] Deressa, C. T., Mussa, Y. O., & Duressa, G. F. (2020). Optimal control and sensitivity analysis for transmission dynamics of Coronavirus. *Results in Physics*, **19**, 103642.

[24] Dror, A. A., Eisenbach, N., Taiber, S., Morozov, N. G., Mizrachi, M., Zigron, A., ... & Sela, E. (2020). Vaccine hesitancy: the next challenge in the fight against COVID-19. *European journal of epidemiology*, **35(8)**, 775–779.

[25] Eryarsoy, E., Delen, D., Davazdahemami, B., & Topuz, K. (2021). A novel diffusion-based model for estimating cases, and fatalities in epidemics: The case of COVID-19. *Journal of Business Research*, **124**, 163–178.

[26] El Mehdi, L., Mehdi, M., Khalid, H., & Noura, Y., (2014), Partial Differential Equations of an Epidemic Model with Spatial Diffusion, *International Journal of Partial Differential Equations*, **2014**, 1–6.

[27] Fudolig, M., & Howard, R. (2020). The local stability of a modified multi-strain SIR model for emerging viral strains. *PloS one*, **15(12)**, e0243408.

[28] Gribaudo, M., Iacono, M., & Manini, D. (2021). COVID-19 Spatial Diffusion: A Markovian Agent-Based Model. *Mathematics*, **9(5)**, 485.

[29] Hethcote, H. W., (2000). The mathematics of infectious diseases. *SIAM Rev*, **42**, 599–653.

[30] Hodgson, S. H., Mansatta, K., Mallett, G., Harris, V., Emary, K. R., & Pollard, A. J. (2021). What defines an efficacious COVID-19 vaccine? A review of the challenges assessing the clinical efficacy of vaccines against SARS-CoV-2. *The lancet infectious diseases*, **21(2)**, 26–35.

[31] Hong, H. G., & Li, Y. (2020). Estimation of time-varying reproduction numbers underlying epidemiological processes: A new statistical tool for the COVID-19 pandemic. *PloS one*, **15(7)**, e0236464.

[32] Iyaniwura, S. A., Rabiu, M., David, J. F., & Kong, J. D. (2022). The basic reproduction number of COVID-19 across Africa. *Plos one*, **17(2)**, e0264455, 1–17.

[33] Kermack W. O., & McKendrick A. G., (1927). A contribution to the mathematical theory of epidemics, *Proc. Roy Soc. London*, **115**, 700–721

[34] Kiamari, M., Ramachandran, G., Nguyen, Q., Pereira, E., Holm, J., & Krishnamachari, B. (2020, November). COVID-19 Risk Estimation using a Time-varying SIR-model. *In Proceedings of the 1st ACM SIGSPATIAL International Workshop on Modeling and Understanding the Spread of COVID-19*, 36–42.

[35] Lauer, S. A., Grantz, K. H., Bi, Q., Jones, F. K., Zheng, Q., Meredith, H. R., Azman, A. S., Reich, N. G. & Lessler, J., (2020). The incubation period of coronavirus disease 2019 (COVID-19) from publicly reported confirmed cases: estimation and application. *Annals of internal medicine*, **172(9)**, 577-582.

[36] MacIntyre, R. (2021). Vaccination for COVID-19 control and considerations for Australia. *Microbiology Australia*, **42(1)**, 30-34.

[37] Madubueze, C. E., Dachollom, S., & Onwubuya, I. O. (2020). Controlling the spread of COVID-19: optimal control analysis. *Computational and Mathematical methods in Medicine*, **2020**.

[38] Mammeri, Y. (2020). A reaction-diffusion system to better comprehend the unlockdown: Application of SEIR-type model with diffusion to the spatial spread of COVID-19 in France.*Computational and Mathematical Biophysics*, **8(1)**, 102–113.

[39] Martnez-Rodrguez, D., Gonzalez-Parra, G., & Villanueva, R. J. (2021). Analysis of key factors of a SARS-CoV-2 vaccination program: A mathematical modeling approach. *Epidemiologia*, **2(2)**, 140–161.

[40] Malinzi, J., Eladdadi, A., and Sibanda, P., (2017), Modelling the spatiotemporal dynamics of chemo-virotherapy cancer treatment, *Journal of Biological Dynamics*,**11(1)**, 244-274.

[41] Malinzi, J., & Quaye, P. A. (2018). Exact solutions of non-linear evolution models in physics and biosciences using the hyperbolic tangent method. *Mathematical and Computational Applications*, **23(3)**, 35.

[42] Malfliet, W., & Hereman, W. (1996). The tanh method: II. Perturbation technique for conservative systems. *Physica Scripta*, **54(6)**, 569–575.

[43] Mondaini, R. P. (2020). *Trends in Biomathematics: Modeling Cells, Flows, Epidemics, and the Environment*. Springer International Publishing.

[44] Moore, S., Hill, E.M., Dyson, L., Tildesley, M.J., & Keeling, M.J. (2021). Modelling optimal vaccination strategy for SARS-CoV-2 in the UK. *PLoS Comput Biol*, **17(5)**: e1008849.

[45] Moore, S. E., Bamen, H. L. N., Asamoah, J. K. K., Menoukeu-Pamen, O., & Jin, Z. (2021). Global Stability and Sensitivity Assessment of COVID-19 with Timely and Delayed Diagnosis in Ghana.

[46] Ministry-Of-Health-Kenya-Covid-19-Immunization-Status-Report-$4^{th}$-June-2022.Pdf

[47] Nyaberi, H. O., & Wakwabubi, V. W. (2020). Mathematical Modeling Of The Dynamics Of Infectious Diseases With Relapse. *Asian Journal of Mathematics and Computer Research*, **27(1)**, 28–37.

[48] Orangi, S., Pinchoff, J., Mwanga, D., Abuya, T., Hamaluba, M., Warimwe, G., Austrian, K., & Barasa, E. (2021). Assessing the level and determinants of COVID-19 vaccine confidence in Kenya. *Vaccines*, **9(8)**, 936–947.

[49] Pontraygin L. S, Boltyanski V., & Mishchenko F., (1962). *The mathematical theory of optimal processes*. Interscience, Berlin.

[50] Pontryagin, L. S. (1987). *Mathematical theory of optimal processes*. CRC press.

[51] Qiu, X., Nergiz, A. I., & Maraolo, A. E. (2020). Defining the role of asymptomatic SARS-CoV-2 transmission: a living systematic review. *medRxiv 2020*, [Google Scholar]

[52] Rappuoli, R., Mandl, C. W., Black, S., & De Gregorio, E. (2011). Vaccines for the twenty-first century society. *Nature reviews immunology*, **11(12)**, 865–872.

[53] Samsuzzoha, M. D. (2012). *A study on numerical solutions of epidemic models* (Doctoral dissertation, PhD thesis), Swinburne University of Technology, Australia, 2012.

[54] Singh, A., Bajpai, M. K., & Gupta, S. L. (2020). A Time-dependent mathematical model for COVID-19 transmission dynamics and analysis of critical and hospitalized cases with bed requirements, *MedRxiv*, 2020-10.

[55] Škraba, A., Vavtar, B., Stanovov, V., Semenkin, E., & Stojanovic, R. (2021). Parametrization of bass diffusion model on COVID-19 first wave data. *In IOP Conference Series: Materials Science and Engineering*, **1047(1)**, 012084.

[56] Tian, B., & Yuan, R. (2017). Traveling waves for a diffusive SEIR epidemic model with standard incidences. *Science China Mathematics*, **60(5)**, 813–832.

[57] Tognotti, E. (2013). Lessons from the history of quarantine, from plague to influenza A. *Emerging infectious diseases*, **19(2)**, 254.

[58] Van-den Driessche, P. & Watmough, J., (2002), Reproduction number and sub-threshold endemic equilibria for compartmental models of disease transmission, *Mathematical Biosciences*, **180(1)**, 29–48.

[59] Wachira, C. M., Lawi, O. G., & Malinzi, J., (2018). A spatiotemporal Model on the Transmission Dynamics of Zika Virus Disease, *Asian Research Journal of Mathematics*, **10(4)**, 1–15.

[60] Wagner, J. G., (1973). Properties of Michaelis-menten equation and its integrated form which are useful in pharmacokinetics, *J.Pharmacokinet. Biopharm*, **1**, 103–121.

[61] Wang, J., Tang, K., Feng, K., Lin, X., Lv, W., Chen, K., & Wang, F. (2021). Impact of temperature and relative humidity on the transmission of COVID-19: a modelling study in China and the United States. *BMJ open*, **11(2)**, e043863.

[62] Wang, J. (2020). Mathematical models for COVID-19: Applications, limitations, and potentials. *Journal of public health and emergency*, **4**.

[63] William, A., David, O., Tenuche, B. S., Samuel, O. K., Alih, D. M., & Johnson, A. (2020). Mathematical Model of the Transmission Dynamics of Corona Virus Disease (COVID-19) and Its Control, *Asian Research Journal of Mathematics*, **16(11)**, 69-88.

[64] World Health Organization (WHO). Corona Virus Disease (COVID-19) Outbreak Situation. *World Health Organization (2020). Available online at: https://www.who.int/emergencies/diseases/novel-coronavirus-2019*

[65] Yu, P., Zhu, J., Zhang, Z., & Han, Y. (2020). A familial cluster of infection associated with the 2019 novel coronavirus indicating possible person-to-person transmission during the incubation period. *The Journal of infectious diseases*, **221(11)**, 1757-1761.

[66] Zamir, M., Abdeljawad, T., Nadeem, F., Wahid, A., & Yousef, A. (2021). An optimal control analysis of a COVID-19 model. *Alexandria Engineering Journal*, **60**, 2875-2884.

[67] Zhen, W., Yamir, M., Stefano, B., & Matjaz, P. (2017). Vaccination and Epidemic in networked populations-An introduction. *Chaos, Solitons and Fractals*, **103**, 177-183

[68] Zhou, Y., Xu, R., Hu, D., Yue, Y., Li, Q., & Xia, J. (2020). Effects of human mobility restrictions on the spread of COVID-19 in Shenzhen, China: A modelling study using mobile phone data. *The Lancet Digital Health*, **2(8)**, 417–424.

## APPENDICES

1. **MATLAB codes for Figure 3.2, (a), (b), and (c)**

```
function dy=M1( ,y)
Lambda=0.00003178; lambda=0.5; beta=varying; eta=0.05; mu=0.0000391;
epsilon=0.2; delta=0.00000103; omega=0.5;
dy=[3000 2000 1500 1000]';
dy(1)=Lambda-(((1-omega)*beta*y(1)*y(3))/(1+eta*y(3)))-mu*y(1);
dy(2)=(((1-omega)*beta*y(1)*y(3))/(1+eta*y(3)))-(epsilon+mu)*y(2);
dy(3)=epsilon*y(2)-(delta+mu+lambda)*y(3);
dy(4)=lambda*y(3)- mu*y(4);
    options=odeset('RelTol',1e-4,'AbsTol',[1e-6 1e-4 1e-6]);
    [T1,Y1]=ode45('M1',(0:0.1:30),[3000,2000,1500,1000]);
    [T2,Y2]=ode45('M2',(0:0.1:30),[3000,2000,1500,1000]);
    [T3,Y3]=ode45('M3',(0:0.1:30),[3000,2000,1500,1000]);
plot(T1,Y1(:,1),'b',T1,Y1(:,2),'g',T1,Y1(:,3),'r','linewidth', 2);
plot(T2,Y2(:,1),'b',T2,Y2(:,2),'g',T2,Y2(:,3),'r','linewidth', 2);
plot(T3,Y3(:,1),'b',T3,Y3(:,2),'g',T3,Y3(:,3),'r','linewidth', 2);
legend('ω = 0.1','ω = 0.5','ω = 0.7');
legend('β = 0.02','β = 0.09','β = 0.5');
legend('Susceptibles','Exposed','Infected');
ylabel 'No. Human Population (S(t), E(t), I(t), R(t))';
xlabel 'Time in days';
```

2. **MATLAB codes for Figure 4.1, 4.2, and 4.3**

```
function value = initial2(x) value = [3000;2000;1500;1000];
function [pl,ql,pr,qr] = bc2(xl,ul,xr,ur,t)
pl = [0;ul(2);0;ul(4)]; ql = [1;0;1;0];
pr = [ur(1);0;ur(3);0]; qr = [1;1;1;1];
function [c,b,s] = eqn2(x,t,u,DuDx)
M=0.00003178; b1=0.02; d=.5; m=0.0000391; g=0.5; h=0.00000103; e=0.05;
```

```
c = [1; 1; 1; 1];
b = [.3; .3; .3; .9999].*DuDx;
F1=(M-((b1*u(1)*u(3))/(1+d*u(3)))-m*u(1));
F2=(b1*u(1)*u(3)/(1+d*u(1)))-(m+e)*u(2);
F3=e*u(2)-(m+g+h)*u(3);
F4=h*u(3)-m*u(4);
s = [F1;F2;F3;F4];
m = 0;
t = linspace(0,40,40);
x = linspace(0,10,80);
sol = pdepe(m,@eqn2,@initial2,@bc2,x,t);
u1=sol(:,:,1);  u2=sol(:,:,2);  u3=sol(:,:,3);  u4=sol(:,:,4);
surf(x,t,u1);  surf(x,t,u2);  surf(x,t,u3);  surf(x,t,u4);
xlabel('Space(km)');
ylabel('Time(days)');
zlabel('Susceptible Humans');
zlabel('Exposed Humans');
zlabel('Infected Humans ');
```

3. **MATLAB codes for Figure 5.3 and 5.4**

```
function dy=M4( ,y)
Lambda=0.00003178;  lambda=0.5;  beta=0.005;  vartheta=0.5, 0.7, 0.9;  beta1=(1-
vartheta)*beta;  eta=0.05;  mu=0.0000391;  epsilon=0.5;  delta=0.00000103;
gamma=0.3, 0.5, 0.9 ;
dy=[500 300 200 150 100]';
dy(1)=Lambda-((beta*y(1)*y(3))/(1+eta*y(3)))-(mu +gamma)*y(1);
dy(2)=gamma*y(1)-((beta*y(2)*y(3))/(1+eta*y(3)))- mu*y(2);
dy(3)=((beta*y(1)*y(3))/(1+eta*y(3)))+((beta1*y(2)*y(3))/(1+eta*y(3)))-(epsilon+mu)*y(3);
dy(4)=epsilon*y(3)-(delta+mu+lambda)*y(4);
dy(5)=lambda*y(4)- mu*y(5);
```

```
options=odeset('RelTol',1e-4,'AbsTol',[1e-6 1e-4 1e-6]);
    [T4,Y4]=ode45('M4',(0:0.01:50),[5000,2000,1500,1200,800]);
    [T5,Y5]=ode45('M5',(0:0.01:50),[5000,2000,1500,1200,800]);
    [T6,Y6]=ode45('M6',(0:0.01:50),[5000,2000,1500,1200,800,0]);
    plot(T4,Y4(:,4),'b',T5,Y5(:,4),'g',T6,Y6(:,4),'r','linewidth', 2);
plot(T5,Y5(:,2),'b',T5,Y5(:,3),'g',T5,Y5(:,4),'r','linewidth', 2);
plot(T6,Y6(:,1),'b',T6,Y6(:,2),'g',T6,Y6(:,3),'r','linewidth', 2);
legend('ϑ = 0.5','ϑ = 0.7','ϑ = 0.9');
legend('γ = 0.3','γ = 0.5','γ = 0.9');
ylabel 'Susceptible Individuals (S)';
ylabel 'Vaccinated Individuals (V)';
ylabel 'Exposed Individuals (E)';
ylabel 'Infected Individuals (I)';
ylabel 'Recovered Individuals (R)';
xlabel 'Time(days)';
```